Spatial distribution and interannual trends of $\delta^{18}O$, $\delta^{2}H$, and deuterium excess in precipitation across North-Eastern Italy

Mauro Masiol [a,*], Daniele Zannoni [a,b], Barbara Stenni [a,c], Giuliano Dreossi [a,c], Luca Zini [d], Chiara Calligaris [d], Daniele Karlicek [d], Marzia Michelini [d], Onelio Flora [d], Franco Cucchi [d], Francesco Treu [d]

[a] Dipartimento di Scienze Ambientali, Informatica e Statistica, Università Ca' Foscari Venezia, IT-30172 Mestre-Venezia, Italy
[b] Geophysical Institute, University of Bergen and Bjerknes Centre for Climate Research, NO-5020 Bergen, Norway
[c] Istituto di Scienze Polari, Consiglio Nazionale delle Ricerche, IT-30172 Mestre-Venezia, Italy
[d] Dipartimento di Matematica e Geoscienze, Università degli Studi di Trieste, IT-34128 Trieste, Italy

ARTICLE INFO

This manuscript was handled by Marco Borga, Editor-in-Chief

Keywords:
Precipitation
Stable isotopes
Deuterium excess
Local meteoric water line
Vertical gradient
Mapping

ABSTRACT

NE Italy presents high-quantity, high-quality and easily exploitable groundwater resources that are seriously threatened by anthropogenic pressures. This study analyzes the oxygen and hydrogen isotopic composition of 2250 precipitation samples collected in 36 sites across the north-easternmost region of Italy, Friuli Venezia Giulia, between 1984 and 2015. This is an unprecedented dataset for North Italy with a high density of sampling sites and a decadal temporal extension. A series of both routine and original chemometric approaches were applied to investigate the temporal and spatial variability of the isotopic composition through relationships with geographical and weather variables. New statistical approaches were presented to model the seasonal and spatial patterns of isotopic composition as well as to summarize the large amount of isotopic data. Significant gradients of $\delta^{18}O$ and $\delta^{2}H$ were detected in the area due to the peculiar orography and climate of the region; the amplitude of the monthly patterns also presented similar gradients. The deuterium excess did not present a clear seasonality, but higher values were found in autumn. The deuterium excess-to-$\delta^{18}O$ ratio exhibited typical patterns throughout the region when grouping the sites for altitude and continentality; in winter, large differences of $\delta^{18}O$ were detected among groups, but deuterium excess remained almost unchanged. The inter-site correlations were moderately high across all the territory even for deseasonalized data. The local meteoric water line (using all the single samples $\delta^{2}H = 7.8 \cdot \delta^{18}O + 8.9$) was also estimated at annual and seasonal basis, evidencing the presence of spatial gradients according to the orographic and weather characteristics of the region. Statistically significant increasing interannual trends (0.23–0.87‰/y) were detected in 11 sites for deuterium excess; the presence of these trends was linked to local processes. Two multiple linear regression models were applied to reconstruct the isotopic composition of precipitation at a regional scale. The stepwise approach returned the best results with root mean square errors in the 0.5-1‰, 3.5–8.2‰ and 0.9–1.5‰ intervals for $\delta^{18}O$, $\delta^{2}H$, and deuterium excess, respectively. The deuterium excess was not modelled in winter, where no relationships were found with geographic variables.

1. Introduction

Water isotopologues undergo temperature-dependent isotope equilibrium exchanges and kinetic non-equilibrium fractionations through all stages of the hydrological cycle. Changes of $^{18}O/^{16}O$ and $^{2}H/^{1}H$ ratios in the atmospheric precipitation are driven by multiple factors besides local temperature, including the moisture source areas as well as climate and weather conditions during evaporation, phase transitions, atmospheric transport pathways, in-cloud processing, and precipitation (Rozanski et al., 1993; Gat, 2010). Consequently, stable isotope ratios of hydrogen and oxygen are widely used in hydrological, climatological, paleoclimatological, environmental, and agricultural studies at global

* Corresponding author at: Dipartimento di Scienze Ambientali, Informatica e Statistica, Università Ca' Foscari Venezia, Via Torino, 155, IT-30172 Mestre-Venezia, Italy.
E-mail address: mauro.masiol@unive.it (M. Masiol).

and regional scales. For instance, water isotopic composition measured in paleoclimate records enables the reconstruction of past climates (Dansgaard et al., 1993; McDermott, 2004; Jouzel et al., 2007; Stenni et al., 2017; Affolter et al., 2019). In modern precipitations, stable water isotopes are used as tracers to investigate the origin of water recharging catchment basins and feeding rivers, aquifers and springs (e.g., Gat, 1996; Mook, 2001; Gat et al., 2001; Rozanski et al., 2001; Geyh et al., 2001; Rodgers et al., 2005; Schulte et al., 2011; Aggarwal et al., 2012; Klaus and McDonnell, 2013; Bowen and Good, 2015) as well as in the study of the hydrological processes of snow (Beria et al., 2018).

The isotope ratios of meteoric waters are commonly expressed as relative deviations to the Vienna Standard Mean Ocean Water (V-SMOW) using the delta notation (Craig, 1961). $\delta^{18}O$ and $\delta^{2}H$ are linked by a strong empirical linear relationship, known as the meteoric water line (MWL). Using worldwide isotope data, Craig, (1961) and Dansgaard, (1964) firstly reported a regression line of $\delta^{2}H = 8{\cdot}\delta^{18}O + 10$, known as the global MWL (GMWL). Beyond the GMWL, many other meteoric water lines have been computed using arithmetic or weighted isotope mean values collected at different time resolutions (e.g. Rozanski et al., 1993; Araguás-Araguás et al., 2000) or using data from specific regions (reported as local MWLs, LMWLs). The regression slope (≈8) primarily reflects the fractionation of the water isotopologues under equilibrium conditions, which is ~ 8-fold stronger for $^{1}H^{2}H^{16}O$ compared to $^{1}H_{2}^{18}O$ (8.6 at 0 °C to 7.7 at 30 °C; Majoube, 1971). The intercept, also known as deuterium excess (d-excess or $d = \delta^{2}H\text{-}8{\cdot}\delta^{18}O$), measures the ^{2}H abundance over ^{18}O (Dansgaard, 1964) with respect to the GMWL. D-excess is known to be sensitive to non-equilibrium fractionation processes driven by the different diffusivity of water isotopologues during evaporation and transition phases (Pfahl and Sodemann, 2014; Benetti et al., 2014; Dütsch et al., 2017). These non-equilibrium effects are favored by peculiar environmental conditions, including strong gradients in relative humidity above the evaporation surface, and fast air mass advection by winds. Under this view, d-excess has been extensively used as a proxy to identify water vapor sources, ocean surface conditions, continental moisture recycling, the evolution of moisture during transport, and plant transpiration (Uemura et al, 2008; Lai and Ehleringer, 2011; Aemisegger et al., 2014; Steen-Larsen et al., 2015).

A first comprehensive study upon the isotopic composition of precipitations across Italy was presented by Longinelli and Selmo (2003). More recently, Giustini et al. (2016) reviewed and summarized most of the published and unpublished data at the national level using annually-averaged data collected over different periods. These studies present an overall view of the isotopic composition of precipitation across Italy but did not account for the strong seasonality linked to climate and weather factors. Both studies mapped the spatial distribution of $\delta^{18}O$ by using nation-wide datasets, i.e. extending over a large domain characterized by different climates. Italy extends over ~ 1150 km in the North-South axis encompassing different climates (Beck et al., 2018). In addition, the Apennine range roughly splits the territory into eastern and western sides, while the Alps enclose the Po Valley to the North. This peculiar orography has a strong effect on the local climate, atmospheric circulation, air mass transport pathways, and on the amount of precipitation (Brunetti et al., 2006; Toreti et al., 2009). Consequently, the isotopic composition of precipitation in Italy is also characterized by a large variability, as reported by Longinelli and Selmo (2003).

A study by Longinelli et al. (2006) reported monthly precipitation samples collected at 12 locations in Northern Italy during 2002–2004, but results were biased by climatological anomalies occurred during the sampling campaign. This study pointed out how possible inter-annual climatological differences may strongly affect the isotopic composition of precipitation. Under this interpretation, studies over the northeastern part of Italy lack of an overall view. For instance, D'Amelio et al. (1994) firstly reported $\delta^{18}O$ in precipitations over Northeast Italy, with data included in the global network of isotopes in precipitation (GNIP). Flora et al. (2009) reported the oxygen isotope composition at 4 sites in the Eastern end of the Po Valley during 2005–2006 to investigate the recharge basin of aquifers. More recently, Cervi et al. (2017) reported the water stable isotopes in one site in the Eastern Alps between 2005 and 2010 to investigate the recharge of aquifers. Zini et al. (2015) and Calligaris et al. (2016) used the stable isotopes values to establish the springs recharge areas for the Mt. Canin cross-border aquifer system (Italy-Slovenia) and for the Mt. Verzegnis aquifer respectively, but the two papers are related only to small areas.

In summary, data on the isotopic composition of precipitation in Northeastern Italy -and more extensively across North Italy- are still sparse and/or incomplete, especially for $\delta^{2}H$ and d-excess. Another main gap is the lack of long-term datasets, a valuable resource for understanding the interannual processes of the water cycle associated with the recent climate variability and change.

To partially fill these gaps, this study presents the isotopic composition of 2250 precipitation samples collected at 36 sites across the north-easternmost region of Italy, Friuli Venezia Giulia (FVG) between 1984 and 2015. Both routine and robust chemometric approaches are applied to summarize the high-density original data presented in this study in a clear and synthetic way. The isotopic data are used: (i) to preliminarily describe the spatial and seasonal variability of the isotopic composition; (ii) to relate water isotopes with orography and weather parameters; (iii) to model the amplitude of seasonal isotopic composition and its dependance on elevation using a seasonal decomposition technique; (iv) to reconstruct the local meteoric water lines across FVG at annual and seasonal bases and investigate their spatial gradients using multiple aggregation approaches; (v) to quantify interannual trends and analyze their spatial distribution using robust nonparametric statistics; (vi) to estimate the spatial distribution of isotope content in precipitation and create annual and seasonal maps with two multiple regression models; and (vii) to match the isotopic composition of modern precipitation with the isotopic composition of groundwater and surface water in the region. The comprehensive set of analysis presented in this study can be easily applied to other areas.

2. Materials and methods

2.1. Study area

The FVG region lies at the north-eastern end of Italy and extends over ~ $7.9{\cdot}10^{3}$ km^{2} encompassing high mountain Alpine environments to the North, intermediate hill zones (the Prealps), and a wide and flat alluvial plain facing the Adriatic Sea to the South. From a hydrogeological point of view, FVG is an interesting case study (Cucchi et al., 2008a; 2008b; Zini et al., 2013). Large highly-permeable carbonate aquifers are present in the Alps and Prealps (e.g., the Classical Karst; Jurkovšek et al., 2016), while the southern part of the region is characterized by an alluvial plain, split by a spring belt into two sectors: the High Plain in the North, characterized by a highly-permeable unconfined aquifer, and the Low Plain in the South, characterized by a system of confined and artesian aquifers (Martelli et al., 2007; Zini et al., 2013). All the aquifers are recharged by strong effective precipitations (peaks > 3000 mm/year), which are higher in autumn (up to 1200 mm during September-November) and lower in spring and summer. The high annual precipitation rate and the lithographical, morphological and hydrogeological characteristics of FVG favor the storage of large amounts of high-quality groundwater in aquifers. This important water resource is today threatened by overexploitation and pollution. Fig. 1 shows the relief map as well as the annual (Fig. 1 and supplementary material S1) and seasonal average precipitation rates in FVG between 2008 and 2015 (Figure S2 and S3).

2.2. Experimental

Most of the data used in this study refer to the 2005/2012 period (Table 1) and are unpublished or reported in a PhD thesis (Michelini,

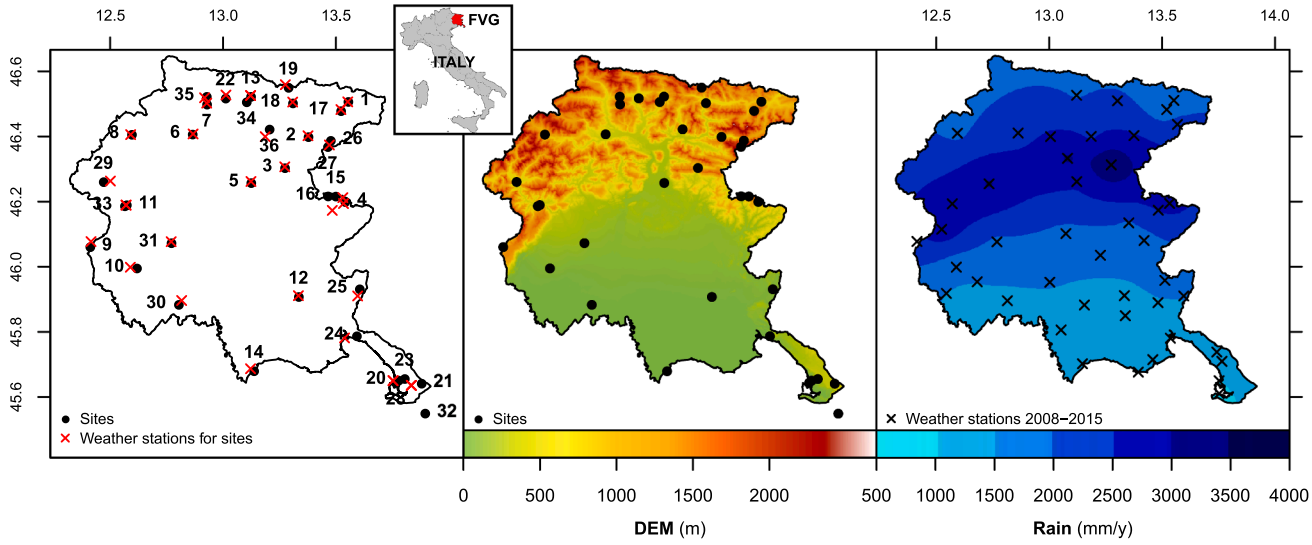

Fig. 1. Map of FVG and sampling sites: (left) location of sampling sites and associated weather stations; (center) relief map showing the digital elevation model data; (right) annual average precipitation rates measured at 44 weather stations managed by the local environmental protection agency (ARPA FVG) during 2008–2015. Rain data are processed by ordinary Kriging; the standard deviation of interpolated rain values is provided in Figure S1.

2013). Some data were already published in Flora et al. (2009), while the isotopic composition of some sites dating back to the 90s was retrieved from D'Amelio et al. (1994), Longinelli and Selmo (2003), and Longinelli et al. (2006). A total of 36 sites have been included in this study (Fig. 1). Table 1 summarizes their general characteristics and sampling periods/frequencies. Sites were selected to fulfil some specifications: (i) data availability must cover at least one year; (ii) samples were collected with monthly to seasonal frequency (Table 1) but the average sampling frequency through all the considered period was less than bimonthly; (iii) the sampling location did not change through the sampling period or, eventually, moved < 1 km from the original location; (iv) the sampling procedures complied with the regulations provided by the International Atomic Energy Agency (IAEA (International Atomic Energy Agency), 2014) for the GNIP network; (v) the analytical protocols were well-established; and (vi) meteorological data (air temperature and rain at ground level) were measured at a nearby weather station located at a distance < 7 km and similar altitude (± 100 m). However, there are some exceptions. Mt. Matajur (ID4, 1326 m) has two nearby weather stations located at a distance < 1.5 km but at different altitudes (1630 m and 907 m); the air temperature was thus derived by averaging the two nearby stations, while the precipitation amount was taken from the station at 907 m (no data for the other one). Rif. Gilberti (ID27) is an Alpine hut at 1848 m equipped with a weather station and has<1 year of available data (May-October 2013). However, it lies close to another site (Sella Nevea, ID26) located at 1170 m, thus it was included in view of assessing the altitude effect. Basovizza (ID21) and Crnotice (ID32) were coupled with the closest weather station located at ~ 3.5 and 10 km, respectively. Sella Nevea (ID26) and Claut (ID29) did not present associated weather data; they are therefore excluded from all the computations requiring meteorological data.

Meteoric water was collected between 1984 and 2015 with monthly-to-seasonal frequencies. Samples were analyzed for $\delta^{18}O$ (all samples), $\delta^{2}H$ and d-excess (1367 samples). Meteoric water samples were collected using rain gauges built to prevent evaporation processes; the newer ones were assembled with the same specifications reported in Gröning et al. (2012), while the older ones used vaseline oil to prevent evaporation, as described in Longinelli et al. (2006); in this latter case, the water samples were carefully syringed out to avoid vaseline contamination. Samples were stored in 50 mL HDPE capped bottles until analysis. The geometry of the rain gauges allows the collection of liquid precipitations. However, precipitation in the form of snow may occur, particularly in high-mountain sites during winter. In this study, no particular precautions were adopted for snow sampling, which was carried out using the same collectors utilized for liquid precipitation, thus the samples during snow periods may undergo some artifacts (e.g., sublimation in the superficial layers accumulated in the funnel, partial melting, and ablation by wind in case of excessive accumulation) due to the snow capping the funnels and the consequent sampling of the snow-melted water.

Oxygen and hydrogen isotopic compositions of most of the samples were determined by the well-established CO_2-H_2/water equilibration method (Epstein and Mayeda, 1953) using automatic equilibration devices (Finnigan MAT HDO 1086) coupled with isotope ratio mass spectrometers (IRMS; Fisons Optima and Thermo-Fisher Delta Plus Advantage). About 5% of samples were analyzed by wavelength-scanned cavity ring-down spectroscopy (CRDS) using a PICARRO model L1102-i. Since the injection of water samples can be affected by between-sample memory effects (Penna et al., 2012), samples were injected 8 times and final results were filtered using an outlier test, i.e. discarding all the results falling outside of the interval described by the average of the 8 repetitions $\pm$ standard deviation.

The analytical precision of IRMS was better or equal to $\pm$ 0.05‰ for $\delta^{18}O$ and $\pm$ 0.7‰ for $\delta^{2}H$; the analytical precision for CRDS was better or equal to $\pm$ 0.10‰ for $\delta^{18}O$ and $\pm$ 0.5‰ for $\delta^{2}H$. The results are reported in the usual delta notation (δ, deltas) and expressed as per mil (‰). Data consistency is discussed in SI section S1.

2.3. Data processing

Statistical and geostatistical analyses were performed using R 3.6.1 (R Core Team, 2019) and a number of packages, including "plyr" (Wickham, 2011), "zoo" (Zeileis and Grothendieck, 2005), "lubridate" (Grolemund and Wickham, 2011), "openair" (Carslaw and Ropkins, 2012), "MASS" (Venables and Ripley, 2002), "reshape" (Wickham, 2007), "car" (Fox and Weisberg, 2019), "DAAG" (Maindonald and Braun, 2019), "boot" (Canty and Ripley, 2019), dunn.test (Dinno, 2017), "relaimpo" (Grömping, 2006), "rgdal" (Bivand et al., 2019), "sp" (Bivand et al., 2013), "raster" (Hijmans, 2019), "gstat" (Pebesma, 2004; Gräler et al., 2016), and "ape" (Paradis and Schliep, 2018).

Samples were collected as close as possible to the end of the month. However, the sample collection was not exactly concurrent at all the sites for logistic and/or weather reasons. Thus, direct comparisons among sites (e.g., correlations, seasonal and trend analyses) were performed on monthly- or annual-averaged data when isotope data cover at

Table 1
Characteristics of the sampling sites and associated weather stations.

ID	Site name	Coordinates[a]		Altitude a.s.l.[b]	Sampling period		Sampling length[c]	Avg. sample duration[d]	Associated weather station[e]	Distance[f]	Diff. Altitude[g]
		Lon	*Lat*	*m*	*Start*	*End*	*months*	*days*		*km*	*m*
1	Tarvisio	13.552	46.51	794	Sep-04	Jun-12	94.3	32	H4 - Tarvisio	0.3	2
2	Saletto	13.376	46.402	496	Sep-04	Feb-11	78.3	33	PCIV - Saletto	0.1	10
3	Musi	13.272	46.306	526	Oct-04	Feb-11	77.1	33	PCIV - Musi	0.1	10
4	Matajur	13.539	46.202	1326	Oct-04	Feb-11	77.1	33	H4 - monte Matajur[i]	1.3	57
5	Gemona	13.122	46.261	184	Sep-04	Jun-12	94.4	34	H4 - Gemona	0.2	0
6	Enemonzo	12.863	46.41	438	Sep-04	Feb-15	125.9	34	H4 - Enemonzo	0.4	0
7	Zoncolan	12.926	46.502	1755	Oct-04	Jun-12	94.1	34	H4 - monte Zoncolan	0.2	5
8	Forni	12.594	46.409	922	Oct-04	Jan-11	76	34	H4 - Forni di Sopra	0.4	0
9	Cansiglio	12.409	46.064	1033	Sep-04	Mar-11	79.6	31	Cansiglio Tramedere[l]	1.6	11
10	Roveredo	12.616	45.998	82	Jul-05	Jan-09	42.7	35	PCIV - Forcate	2.1	15
11	Barcis	12.571	46.193	460	Jul-05	Jan-11	66.5	33	H4 - Barcis	0.4	8
12	Palmanova	13.333	45.91	29	Jul-05	Dec-14	115.1	35	PCIV - Palmanova	0.1	0
13	Paularo	13.121	46.526	633	Jul-05	Feb-11	67.5	33	PCIV - Paularo	0.1	9
14	Lignano	13.135	45.682	15	Dec-06	Oct-10	46.5	41	PCIV - Lignano Sabbiadoro	1.2	0
15	Pojana	13.497	46.219	220	Feb-06	Jun-09	40.1	32	PCIV - Pulfero	5.2	35
16	Mt. Mia	13.463	46.22	969	Nov-07	Jun-09	18.9	32	PCIV - Montemaggiore	6.1	62
17	Mt. Lussari	13.52	46.482	1760	Jun-06	Jul-12	66	32	H4 - monte Lussari	0.2	0
18	Pontebba	13.307	46.506	559	Apr-06	Jun-12	76	34	PCIV - Pontebba T.P.	0.1	9
19	Pramollo	13.288	46.553	1537	Apr-06	Jun-12	76	37	PCIV - Passo Pramollo	1.2	7
20	Trieste via Filzi	13.775	45.654	14	Apr-06	Dec-15	118.2	34	Trieste molo F.lli Bandiera	1.8	14
21	Basovizza	13.877	45.644	400	Apr-86	Dec-15	361.7	38	PCIV - Trieste Cattinara	3.6	135
22	Rivo	13.009	46.52	600	Jan-90	Oct-15	314.4	36	PCIV - Paluzza	0.9	18
23	Trieste Lab	13.802	45.658	86	Nov-11	Oct-14	35.7	33	PCIV - Trieste Cattinara	3.5	46
24	Randaccio	13.59	45.79	16	Jun-12	Jan-15	31.6	32	H4 - Monfalcone	4.2	16
25	Gorizia	13.603	45.934	63	Jun-12	Jan-15	31.7	33	PCIV - Gorizia Aereoporto	2.7	10
26	Sella Nevea	13.475	46.39	1170	Nov-12	Jan-15	26.2	35	Not available[l]	–	–
27	Rif. Gilberti	13.462	46.371	1848	May-13	Dec-13	5.4	32	PCIV - Livinal Lunc	0.7	11
28	Trieste Nautico	13.764	45.647	20	Jan-84	Oct-12	350	36	Trieste molo F.lli Bandiera	1	20
29	Claut	12.469	46.264	558	Jan-05	Dec-06	23.7	32	Not available[m]	–	–
30	Chions	12.802	45.886	20	Jan-05	Dec-06	23.7	30	H4 – S. Vito Tagliamento	1.6	1
31	Vivaro	12.769	46.076	142	Jan-05	Dec-06	23.7	30	H4 - Vivaro	0.2	0
32	Crnotice	13.893	45.552	384	Feb-08	Mar-09	13.4	33	PCIV - Trieste Cattinara	10.4	119
33	Barcis2	12.563	46.189	424	Jan-05	Feb-07	25.4	31	H4 - Barcis	0.6	44
34	Paularo2	13.102	46.509	990	Nov-05	Nov-06	12.3	37	PCIV - Paularo	2.4	348
35	Ravascletto	12.925	46.526	981	Nov-05	Nov-06	12.5	37	PCIV - Ravascletto	0.9	68
36	Pradis	13.203	46.425	402	Jun-98	Apr-06	95.4	56	PCIV - Moggio Udinese	3.1	92
	Total[h]	–	–	544	–	–	–	35	–	–	–

(a) Coordinate system: WGS84; (b) a.s.l. = above sea level; (c) number of sampling months; (d) average duration of single samples collected over the entire sampling period; (e) name of the weather stations used for retrieving meteorological data; (f) distance between sampling sites and the associated weather stations; (g) altitude difference between sampling sites and the associated weather stations; (h) average of the entire set of collected samples; (i) weather station managed by ARPA Veneto; (l) no associated weather stations at a distance < 10 km with altitude difference < 100 m or no weather data; (m) a weather station is close to the sampling site, but periods of available weather data do not correspond to the isotope data.

Table 2
LMWLs computed on aggregated data. Confidence intervals (CI) were computed using ordinary nonparametric bootstrap resampling (2000 replicates). RMSE = root mean squared error; MAE = mean absolute error. LMWLs for single sites are reported in Table S3.

		Intercept		Slope		r^2	CV RMSE	CV MAE
Data aggregation	Period	β_0 (±std. error)	BS 95th CI	β_1 (±std. error)	BS 95th CI		(‰)	(‰)
Single samples								
	Entire dataset	8.87 (±0.26)	[8.27;9.43]	7.8 (±0.03)	[7.73;7.87]	0.98	3.1	2.5
	Winter	13.5 (±0.53)	[12.52;14.55]	8.31 (±0.05)	[8.21;8.41]	0.99	2.8	2.2
	Spring	6.17 (±0.57)	[5.03;7.21]	7.56 (±0.07)	[7.41;7.69]	0.97	2.7	2.1
	Summer	4.04 (±0.51)	[2.87;5.2]	7.09 (±0.08)	[6.9;7.28]	0.96	2.5	2.0
	Autumn	10.3 (±0.55)	[9.04;11.72]	7.75 (±0.06)	[7.6;7.92]	0.98	3.1	2.2
Aggregated samples								
Unweighted	Single years averages	6.14 (±0.97)	[4.28;7.86]	7.46 (±0.12)	[7.22;7.67]	0.98	1.6	1.3
Precipitation-weighted	Single years averages	5.3 (±1.07)	[3.14;7.33]	7.29 (±0.13)	[7.02;7.56]	0.97	1.5	1.2
Temperature weighted	Single years averages	2.61 (±1.65)	[-1;5.54]	6.83 (±0.24)	[6.26;7.28]	0.90	2.0	1.5
Unweighted	Yearly averages	6.24 (±1.44)	[3.98;8.56]	7.45 (±0.18)	[7.14;7.75]	0.99	1.4	1.1
Precipitation-weighted	Yearly averages	4.89 (±1.70)	[2.14;8.14]	7.23 (±0.21)	[6.85;7.66]	0.98	1.3	1.0

least 95% of days in a month or year, respectively. Beside arithmetic averages, isotope data are also reported as precipitation-weighted averages using the amount of water measured in the sampling collectors. A few data missed this information; thus, the water amount was reconstructed by regressing the rainfall from the weather stations on the available data. A good relationship ($r^2 = 0.85$) was found, indicating that the reconstructed water amount can be used.

In simple and multiple linear regression models, the 95th percentile confidence intervals (CI) in the prediction of the slopes and intercepts were computed by ordinary nonparametric bootstrap resampling (Davison and Hinkley, 1997) over 2000 replicates. In addition, the measure of performance and predictive ability for regression models were estimated by *k*-fold cross-validation (Maindonald, and Braun, 2010; James et al., 2013), which randomly partitions the datasets into *k* ($k = 5$, in this case) equal-sized subsamples and recursively uses *k*-1 parts to re-fit the regression and the remaining part as a testing set. The root mean squared error (RMSE) and mean absolute error (MAE) obtained from residuals of original and cross-validated models were used as a quantitative measure of errors associated with the estimates.

The seasonal patterns were analyzed by applying a seasonal-trend decomposition time series procedure based on 'loess' (STL; Cleveland et al., 1990) aiming to decompose time series into seasonal patterns, inter-annual trends, and residuals. STL uses a local regression smoothing, thus smooth estimates are calculated for all possible time values. Since STL cannot handle missing data, a reconstruction based on seasonal Kalman filter (Zeileis and Grothendieck, 2005) was applied before STL analysis. The STL analysis was performed in the 'robust mode', as some variables are not normally distributed (Shapiro-Wilk test at $p < 0.05$). Since this procedure aims to model the seasonal pattern, the window parameter was set as "periodic", thus no changes in seasonality were allowed. Confidence intervals (95%) for trends and seasonality were assessed by bootstrap resampling over 2000 replicates.

Inter-annual monotonic trends were computed through the Mann-Kendall trend analysis (Mann, 1945; Kendall, 1975) and the Theil-Sen nonparametric estimator of slope (Theil, 1992; Sen Pranab Kumar, 1968). This method provides the median of the slopes of all lines through pairs of points using a robust regression technique which is fairly insensitive to outliers; the uncertainty and *p*-values of these trends were estimated by also accounting auto-correlation and using block bootstrap simulations (block length set to 1/3th the length of the time series).

The scientific literature reports a number of different methods to map the isotopic compositions of precipitation (e.g., Bowen and Wilkinson, 2002; Dutton et al., 2005; Liebminger et al., 2006a; van der Veer et al., 2009; Lykoudis et al., 2010; Delavau et al., 2011; Holko et al., 2012). In this study, the spatial distributions of $\delta^{18}O$, $\delta^{2}H$, deuterium excess and their precipitation-weighted values were estimated at annual and seasonal basis according to two strategies and using isotope data collected over periods < 60 days. These two models have the advantage to be simple, including 3 or 4 variables and linear relationships; they were selected to obtain a quick prediction of the isotopic composition of precipitation across the region. Methods are comprehensively presented in SI section S2. Briefly, the first method adopts a stepwise regression analysis and uses the Akaike information criterion as an estimator of the relative quality of statistical models. An additional variable (T_{diff}) was added to account for the difference between the average air temperature during each sampling period and the average air temperature recorded in the same period for a reference 3 year-long period (January 2013 to December 2015). The second method was performed for comparison with Giustini et al. (2016) and was developed upon 3 steps, similarly to Bowen and Wilkinson (2002).

The presence of spatial patterns in the residuals of both methods was investigated by applying the inverse distance squared weighted interpolation (IDW, power 2) and was reported along with the results. This deterministic method was preferred over others, e.g., Kriging and thin-plate spline because residuals should be uncorrelated to other independent variables, i.e. the spatial pattern of residuals is supposed to be driven by local variations, which cannot be captured (modelled) by looking at neighborhood points without assuming random or deterministic spatial variations.

3. Results and discussion

A summary of all collected samples is reported in Table S1, while data distributions are provided as boxplots in Fig. 2 (annual) and Figure S4 (seasonal). The isotopic composition shows a large variation among sites and among seasons. Considering all the single samples collected over the entire study period, $\delta^{18}O$ ranged from −21.6‰ to −1.7‰, while $\delta^{2}H$ varied from −155‰ to −13‰ and deuterium excess from −0.9‰ to 24.6‰. The average air temperature corresponding to the period covered by every single sample was in the −9/+26 °C range.

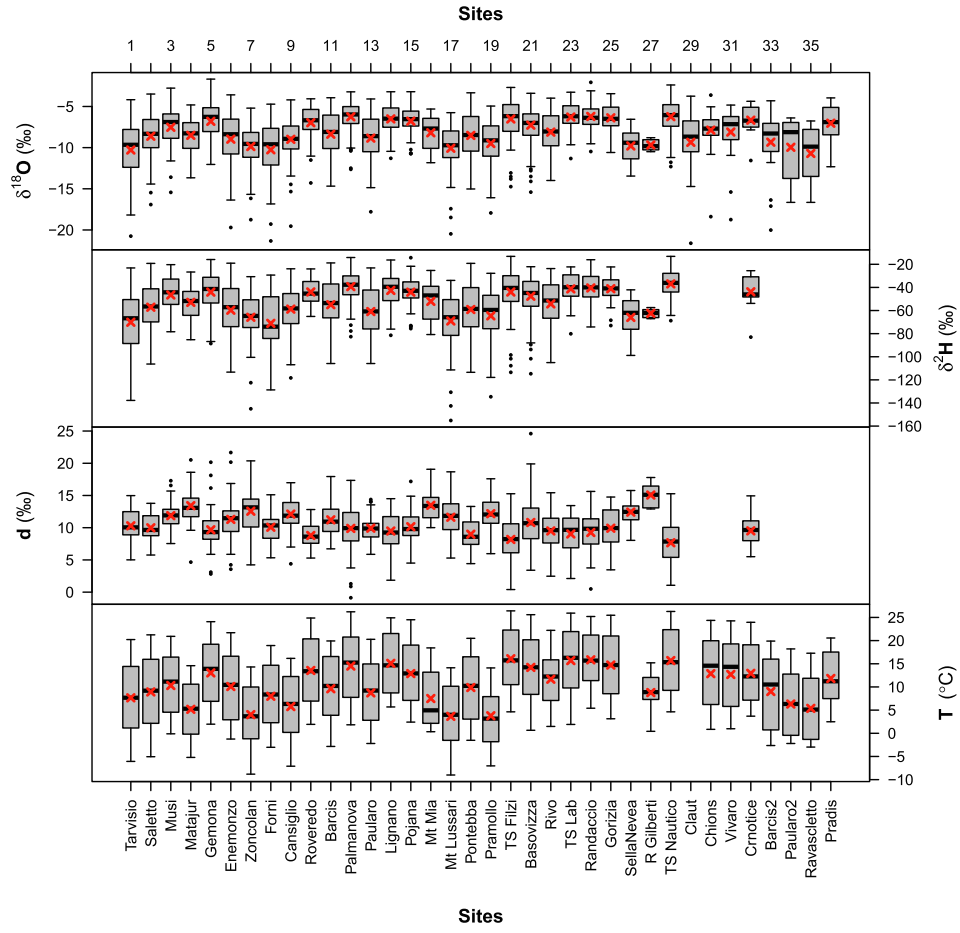

Fig. 2. Boxplots showing the distribution of all isotope data at the 36 sites as well as the distribution of air temperature measured at the nearest weather stations (Table 1) (line = median, box = inter-quartile range, whiskers=±1.5*inter-quartile range, dots = outliers and extremes; red cross = arithmetic mean).

3.1. *Weather-dependence and seasonality of $\delta^{18}O$ and $\delta^{2}H$*

The lower delta values were generally recorded during the colder periods and in sites located at higher altitudes. The known positive relationship between the isotopic composition of precipitation and air temperature (commonly known as *temperature effect*; Dansgaard, 1964; Rozanski et al., 1993) is mainly observed at high and mid-high latitudes. The relations between air temperature and $\delta^{18}O$ or $\delta^{2}H$ are uniform across the region, considering both the average air temperature (T; Fig. S5-6) recorded during each sampling period and the precipitation-weighted air temperature (T_p; Figures S7-8), calculated to account for the different precipitation rates possibly recorded over the study area and during different seasons (Fig. 2 and Figure S2). However, these relations exhibit very variable squared correlations (r^2) amongst sites. The regression slopes for sites with $r^2 \geq 0.5$ ranged from 0.28 to 0.53 $\delta^{18}O$ ‰/°C_p and from 1.8 to 4.2 $\delta^{2}H$‰/°C_p. The temperature effect was not related to the site altitude (Figure S9a) but exhibited a spatial gradient with higher values toward the northern sites (Figure S9b). The intercepts, indicating the delta values expected at 0°C_p, were in the −10/-14‰ and −70/-100‰ for $\delta^{18}O$ and $\delta^{2}H$, respectively. The intercepts showed a spatial gradient similar to the slopes with more depleted isotopic composition of precipitations toward the northern and more continental areas (Figure S9c). These spatial patterns can be attributed to the interplay of several known effects driving the isotope fractionation (e.g., cumulative effects of the Rayleigh fractionation processes during the transport of air masses from moisture sources, possible different moisture source areas or atmospheric transport pathways, cloud processes, etc.) (Christner et al., 2018). In addition, possible artefacts due to snow sampling and accumulation in rain gauges may affect these results, particularly in the high-mountain sites, as snow is generally more depleted in the heavier isotopes than rain (Beria et al., 2018). Under this view, Figures S5-8 clearly show that the linearity of the relationships between air temperature and $\delta^{18}O$ or $\delta^{2}H$ was often broken up by some samples mostly collected in winter and transition periods exhibiting particularly depleted delta values. These samples may reflect the effect of the precipitation in the form of snow.

The relationship with air temperature at a regional level was investigated by considering the annual precipitation-weighted deltas ($\delta^{18}O_p$ and $\delta^{2}H_p$) and the data averaged over all the study period (including round years having at least 95% of available isotope data). Surface air temperature was able to explain 77% of the $\delta^{18}O_p$ and 63% of $\delta^{2}H_p$ variances (Fig. 3 and Table S2). The slopes were 0.24 [CI 0.2–0.3] $\delta^{18}O_p$‰/°C and 1.7 [CI 1.2–2.1] $\delta^{2}H_p$‰/°C. Similar values were obtained using the precipitation-weighted air temperature (Table S2).

The isotopic composition is also influenced by altitude (*altitude effect*). This temperature-related effect combines (i) the increased equilibrium fractionation following the adiabatic cooling with the altitude and (ii) the increasingly stronger depletion of heavier isotopes due to temperature-dependent distillation process during the uplift of air masses. Consequently, the most negative delta values were generally recorded in high-altitude sites (Fig. 3), as already reported in the Alpine area (Liebminger et al., 2006b). Annually, site altitude explains 71% and 61% of $\delta^{18}O_p$ and $\delta^{2}H_p$ variances with vertical isotopic gradients of −0.17 [CI −0.23 and −0.14] $\delta^{18}O_p$‰/100 m and −1.3 [CI −1.8 and −0.9] $\delta^{2}H_p$‰/100 m (Table S2), which are compatible with previous data collected in FVG (-0.19 $\delta^{18}O$‰/100; Longinelli and Selmo, 2003) and North Italy (−0.22 $\delta^{18}O$‰/100; Giustini et al., 2016).

The temperature effect mostly drives the monthly patterns, which

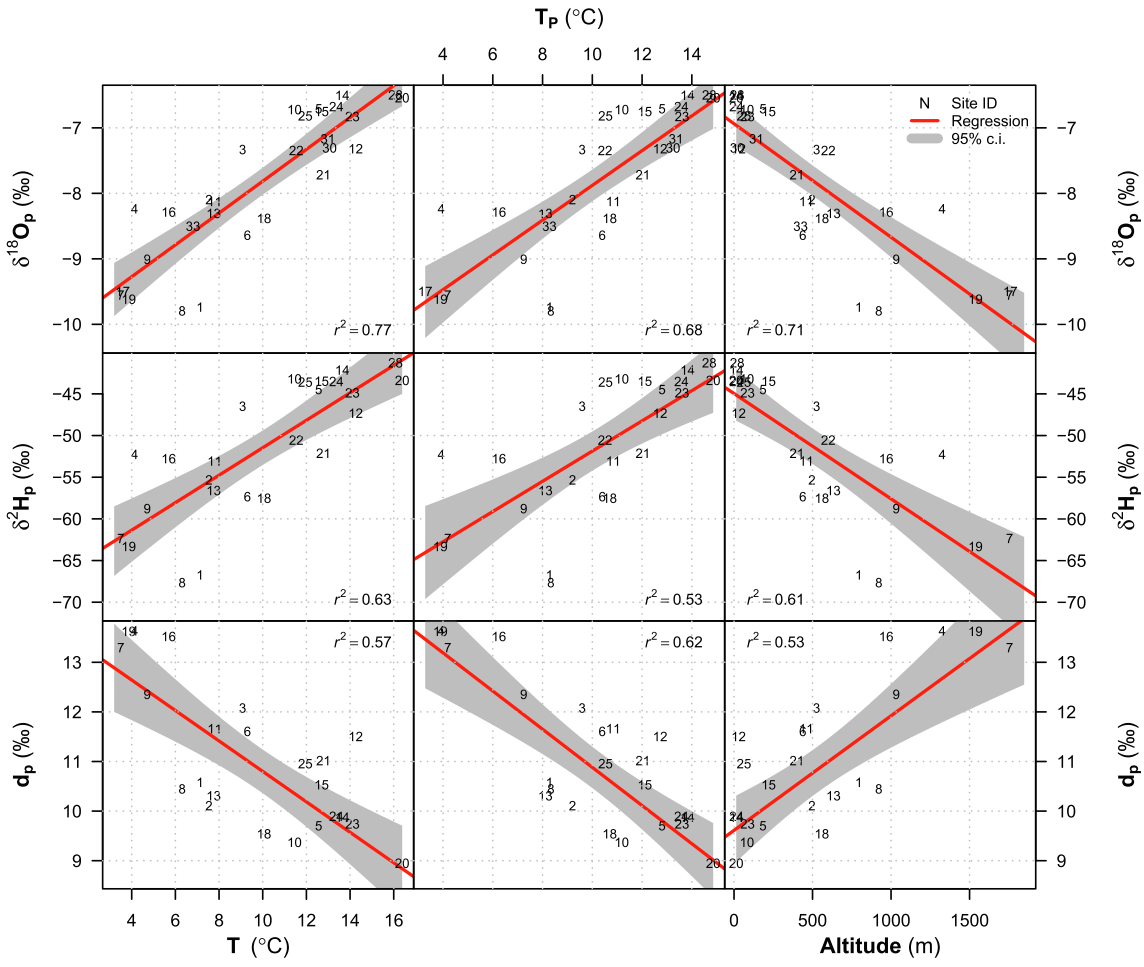

Fig. 3. Linear regression analysis between precipitation-weighted delta values and d-excess against air temperature (T), precipitation-weighted air temperature (T_p), and site altitude using annually-averaged data. The numbers show each site ID (Table 1). Regression statistics are reported in Table S2.

exhibit more depleted values in winter and the less depleted deltas in summer (Fig. 4 and S4), as reported in other studies close to the FVG (e.g., Vreča et al., 2006; 2011; 2014; 2015). Since the seasonal variations of $\delta^{18}O$ and $\delta^{2}H$ are almost homogeneous across the study area, the seasonal patterns of the isotopic composition were analyzed through STL by decomposing the time series into interannual trends and periodic detrended seasonal patterns with 12-month time windows. Results showed quasi-sinusoidal seasonal cycles at all the sites. Considering the 95th percentile CI computed by bootstrap resampling, the amplitude of the seasonal component was lower at the sites located in the southernmost areas, i.e. close to the coastline or in the lower plain (Fig. 5a;b and Figures S10 and S11).

Although the resulting periodic seasonality of the STL is not a perfect sinusoidal curve, the amplitudes were calculated as half the difference between the maximum and minimum in the seasonal patterns. The average interannual trend and the amplitude of the de-trended seasonal components were then investigated to depict their spatial variation. Ordinary Kriging was used to interpolate the data after evaluating semivariograms and residual analysis. The interannual trend components represent the deseasonalized time series; their averages are therefore roughly comparable to the mean values recorded during the sampling campaign. Consequently, results point out again that there is a vertical gradient with more depleted isotopic values at higher latitudes (Fig. 6 and S12), which roughly correspond to sites located at higher altitudes due to the peculiar orography of FVG. Similarly, amplitudes showed a gradient with increasing values at higher latitudes. Thus, the amplitude of time series due to the seasonal effect increases according to the degree of the isotopic depletion. A similar result was reported by Jódar et al. (2016), who analyzed the changes in the seasonal isotopic amplitude of precipitations collected along a vertical transect in a central Alpine region (Switzerland, at altitudes between 250 and 2020 m a.s.l.). This latter study used a different approach to model the seasonal patterns (a general sinusoidal function) and found that (i) the isotopic amplitude depends upon the elevation if the air moisture sources are common, and (ii) the amplitude also depends on local evaporation controlled by local atmospheric and synoptic conditions. Similarly to Jódar et al. (2016), statistically significant linear relationships were found between the site altitude and the amplitude of $\delta^{18}O$ ($r^2 = 0.62$) and $\delta^{2}H$ ($r^2 = 0.63$) (Fig. 5c;d), when excluding the 5 sites located above 1000 m a.s.l. (ID 4, 7, 9, 17, 19). These high-mountain sites show isotopic seasonal amplitudes smaller than expected given their elevations. This effect can be explained by the increased inter-seasonal ranges of air temperature recorded at higher locations as well as by other factors influencing the isotopic composition, such as the closeness to sources of water moisture (Gat et al., 2003). In addition, the effect of possible artefacts in sampling due to the snow accumulation in the rain gauges may have affected the results.

The *amount effect*, related to the quantity of precipitation, was not detected for any variable both considering the amount of water sampled at each site (Figures S13-S14) or the rain amount measured by the corresponding weather stations. Similarly, no relationships were found with relative humidity.

3.2. *Weather-dependence and seasonality of deuterium excess*

On the contrary, the air temperature had a weak and non-uniform

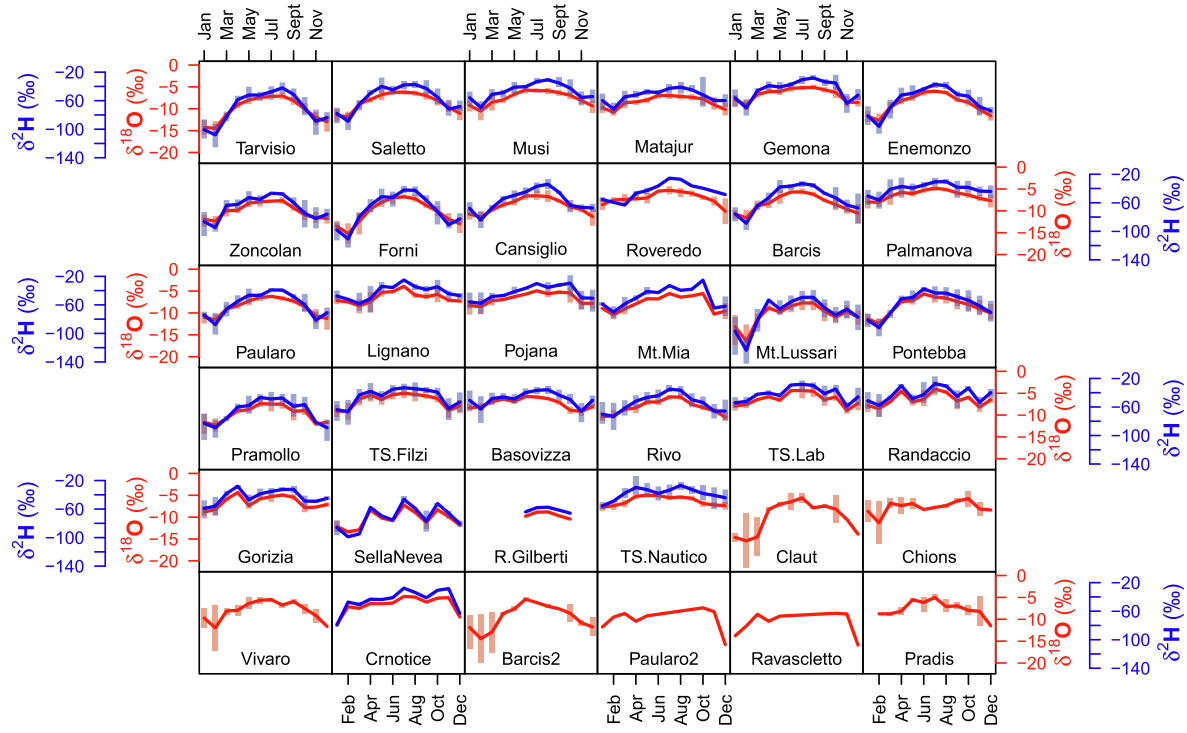

Fig. 4. Monthly patterns for $\delta^{18}O$ (red) and $\delta^{2}H$ (blue). The lines represent the averages; the bars are the 95th confidence intervals in the mean. The monthly patterns for d-excess are reported in Figure S17 (for interpretation of the references to color in the figure, the reader is referred to the web version of this article).

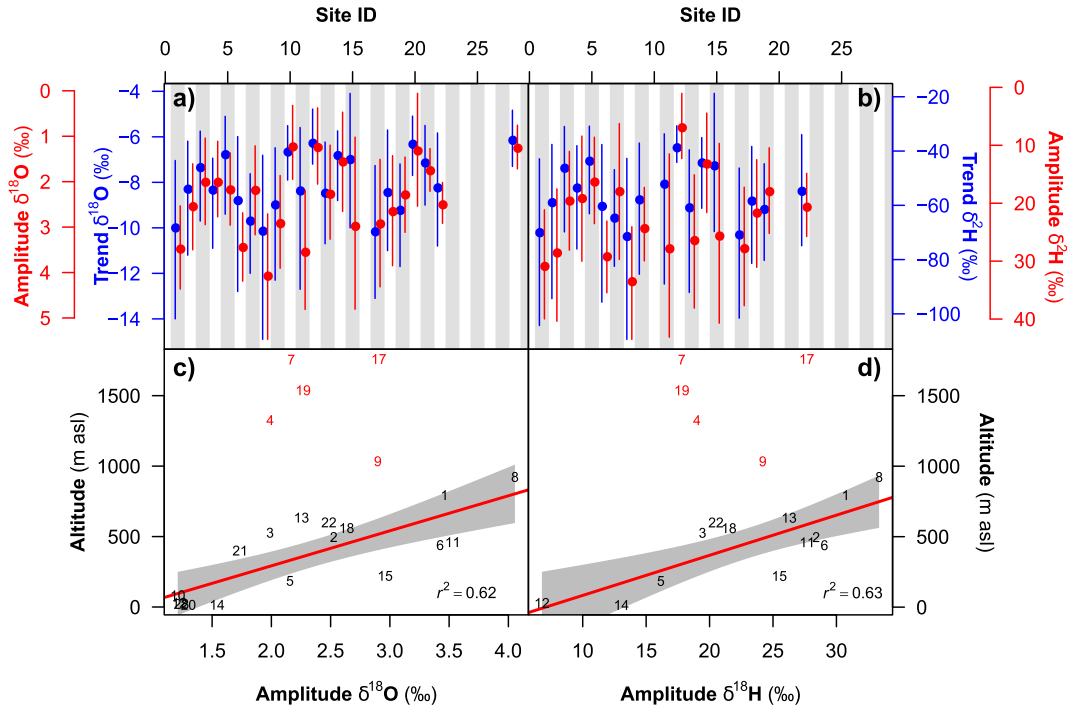

Fig. 5. Average trends (blue dots) and the amplitudes (red dots) obtained by the STL analysis for $\delta^{18}O$ (a) and $\delta^{2}H$ (b) and linear relationships between site altitude and the amplitudes (c, d). In (a, b),bars correspond to the min–max range of the average trends and the 95th confidence intervals of the amplitudes computed by bootstrapping (2000 replicates). In (c, d), the linear relationships (red lines) and their 95th confidence intervals (grey) are reported; the 5 sites located above 1000 m asl (ID 4, 7, 9, 17, 19) are shown in red (for interpretation of the references to color in this figure, the reader is referred to the web version of this article).

effect on deuterium excess when considering all single sample data (Figure S4, S15-S16). The regression computed using annually averaged data showed moderate ($r^2 \approx 0.6$) relationships of −0.38 [CI −0.46;-0.28]‰/°C_p, which is the mirror image of those for $\delta^{18}O$ and $\delta^{2}H$ (Fig. 3). Using the data from the GNIP network, Froehlich et al. (2002) reported that deuterium excess in the Northern Hemisphere exhibits lower values in summer and higher in winter. In this study, the seasonal cycles were highly variable, often with no recognizable patterns

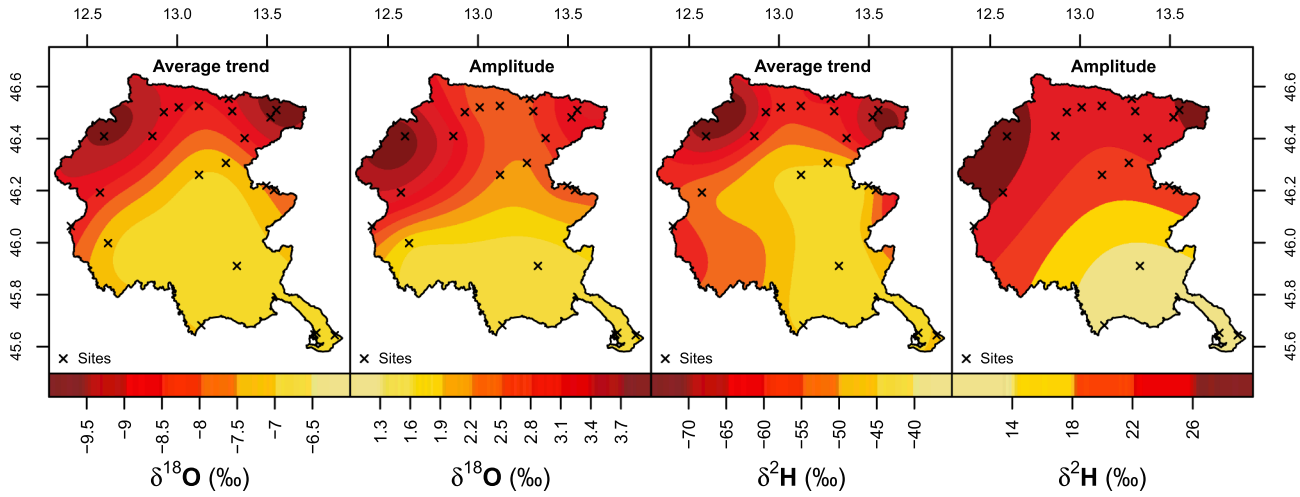

Fig. 6. Maps showing the spatial variation of average trends and amplitudes computed through STL analyses and predicted by ordinary Kriging interpolation. The Kriging relative standard error maps are reported as Figure S12. The maps also report the sites included in the computations (black crosses), which may differ between $\delta^{18}O$ and $\delta^{2}H$ because of data availability.

(Figure S17) and STL decomposition failed to detect a periodic seasonal component for almost all the sites. However, higher values were generally recorded in autumn and minima during spring-summer. Similar patterns are reported in Alpine areas surrounding FVG (Liebminger et al., 2006b; Hager and Foelsche, 2015) and other countries facing the Northern Adriatic Sea (e.g., Vreča et al., 2006; 2007; 2015; Bronić et al., 2020). The relationship with altitude was 0.23 [CI 0.15;0.3] ‰/100 m ($r^2 = 0.53$). No statistically significant effects were recorded for the amount of precipitation (Figure S18) neither for relative humidity.

The altitude effect and the seasonal cycles of d-excess were then jointly analyzed with $\delta^{18}O$ by using the precipitation-weighted seasonal averages for pairs of sites located at different altitudes and at a distance < 10 km. The selected pairs were Tarvisio-Mt. Lussari (altitude difference ΔH 966 m), Pontebba-Pramollo (ΔH 978 m), Enemonzo-Zoncolan (ΔH 1317 m), Trieste Filzi-Basovizza (ΔH 314 m), Sella Nevea-Rif. Giberti (ΔH 678 m, only summer data), and Pojana-Matajur (ΔH 1106 m), which also has an intermediate site (Mt. Mia). Beyond the seasonal patterns (more ^{18}O-depleted values in winter and higher deuterium excess in autumn) and the altitude effect (more ^{18}O-depleted values and higher deuterium excess in mountain sites), results also show that the seasonal variations of $d_p/\delta^{18}O_p$ follow anticlockwise "cycling patterns" (Fig. 7a). The pattern was detected at almost all the pair of sites; thus, it can be considered homogeneous throughout the study area.

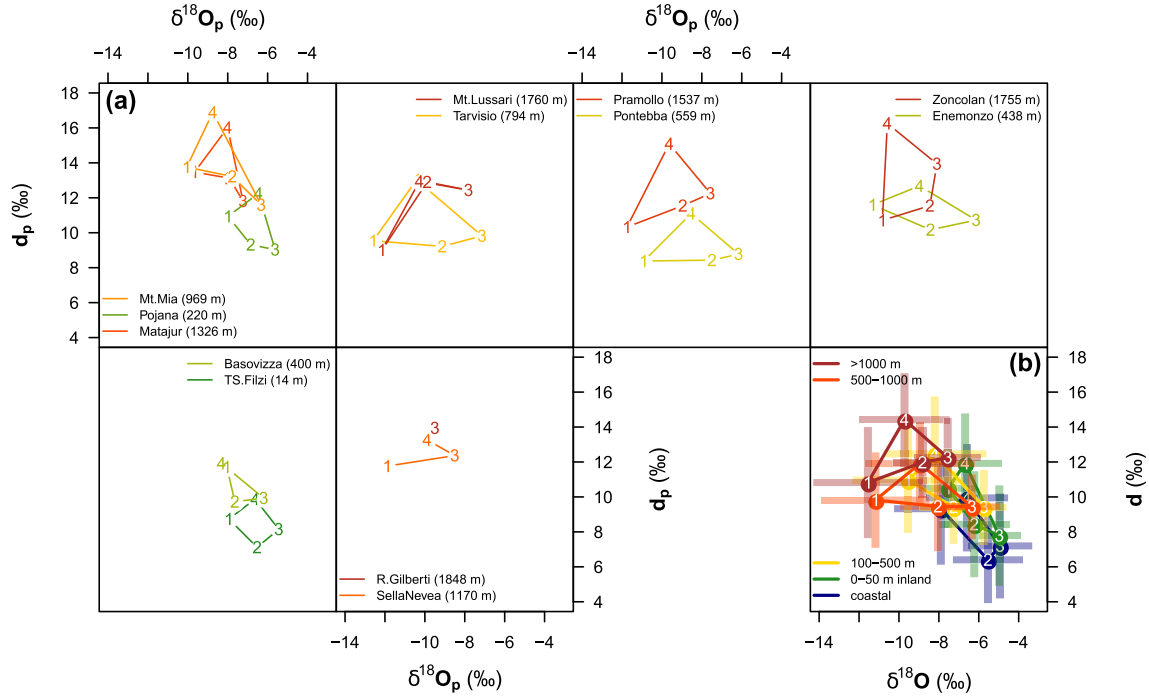

Fig. 7. (a) Relation between the precipitation-weighted seasonal averages of $\delta^{18}O$ and d-excess for pairs of sites located at different altitudes but at a distance < 5 km; (b) relation between $\delta^{18}O$ and d-excess measured on single samples categorized by seasons and clustered for sites located in 5 altitude groups (site ID for group 1 "coastal" 20, 24, 28; group 2 "0–100 m inland" 10, 12, 14, 23, 25; group 3 "100–500 m" 2, 5, 6, 11, 15, 21, 32; group 4 "500–1000 m" 1, 3, 8, 13, 16, 18, 22; group 5 ">1000 m" 4, 7, 9, 17, 19, 26). The seasons are listed as: winter (1), spring (2), summer (3), and autumn (4) (for interpretation of the references to color in the figure legend, the reader is referred to the web version of this article).

Generally, the transition between winter and spring exhibited high changes of $\delta^{18}O_p$ but small variation of d_p in the more continental sites. On the contrary, an opposite behavior was recorded between spring and autumn, exhibiting similar $\delta^{18}O_p$ values against higher changes of d_p. For $\delta^{18}O$, this result reflects the cumulative effect of equilibrium fractionation of atmospheric vapor when air moves from the sea to more continental areas as well as the result of temperature changes due to the adiabatic cooling of the air with the altitude. For d-excess, this pattern probably reflects the increasingly higher effect of non-equilibrium fractionation due to evapotranspiration, large-scale advection of water vapor evaporated in remote source areas as well as the effect of local boundary layer dynamics. Another explanation could be related to the interaction between falling raindrops and orographic clouds (*seeder-feeder mechanism*) that may have a relevant effect on d-excess (Liotta et al., 2006a). This mechanism occurs when precipitation droplets or ice particles from an upper-level cloud (seeder) falls through a lower-level cloud formed by orographic lifting (feeder). The result is an enhancement of the orographic precipitation since the feeder clouds could be washed out by the falling precipitation through collision, coalescence or aggregation processes. However, the interpretation of d-excess patterns is often ambiguous because of changes in water vapor sources and vapor transport which may affect d in non-unique ways (Bershaw, 2018).

In addition, Fig. 7a also shows that the cycles do not overlap for most of the pairs, indicating that both the equilibrium and kinetic fractionations may occur locally rather than reflecting air masses of different origin or history (due to the closeness of the pair of sites). Under this view, the topography plays a key role in determining microclimatic changes in the Alpine areas (Beniston, 2006), especially due to altitude, slope profile, aspect, the orientation of slopes with respect to the prevailing wind regimes, and solar irradiation exposure. The topographical factors have a strong impact on the distribution of precipitations as well as on their isotopic composition. These effects include: (i) the increased fractionation following the adiabatic cooling with the altitude, (ii) the progressive effects of the Rayleigh distillation when air masses from the sea to the more continental areas, thus from the sea (the main source of water vapor) throughout the Alpine areas, (iii) the progressive isotopic fractionation when precipitation falls on the windward-facing slopes of the mountains during uplift, and (iv) the mixing of different water vapor sources and post-condensation evaporation and evapotranspiration.

The $d/\delta^{18}O$ patterns were also investigated by using all single monthly samples and by grouping the sites by altitude and continentality (Fig. 7b). Generally, the more elevated and continental the sites are, the more ^{18}O-depletion and higher d values the samples show. This relationship is observed during all the seasons but winter, which shows large changes of $\delta^{18}O$ within groups accompanied by almost constant values of d-excess. This result indicates that non-equilibrium fractionation processes during winter are almost constant over all the study area. This finding might be partially explained by the different origin of air masses during the year, with the Atlantic provenance dominating the air mass origin on the study area during winter (Sodemann and Zubler, 2010).

3.3. Inter-site comparisons

The monthly data collected at all single sites were analyzed to detect the pairwise inter-site correlations and inter-site differences using nonparametric statistics. The correlation on ranks was measured by the Spearman' rho. Almost all the pairs of sites were significantly ($p < 0.05$) and moderately ($0.4 < \rho < 0.6$) to highly ($\rho > 0.6$) correlated (Figures S19-21, bottom-left). However, the bivariate correlations measured on variables undergoing similar periodic cycles mostly reflect the concurrent effect of the seasonal patterns. To overcome this limitation, the monthly data were normalized by subtracting the average values computed over the four seasons. The correlation matrixes using "deseasonalized" time-series (Figures S19-21, upper-right) still showed significant and moderate to high correlations, indicating that the month-to-month isotopic composition varied almost uniformly over the entire study domain nevertheless the site characteristics and location in the study area. This result is consistent with similar source areas and air mass pathways for all the sites.

3.4. Local meteoric water lines

The LMWLs, revealing the linear relationship between $\delta^{18}O$ and $\delta^{2}H$, were determined by considering all single samples from the entire study period (Fig. 8) as well as using aggregated data (Figure S22). Unweighted and precipitation-weighted aggregated data were computed either considering entire years (Jan to Dec) with at least 95% of sampled days (single-year averages; Figures S22a-c) and the average of all available entire years (multi-year averages; Figures S22d-e). Regression statistics are summarized in Table S3; the coefficients were always statistically significant at $p < 0.05$. The LMWLs determined over unweighted year averages ($r^2 = 0.98$; Figure S22d) was:

$$\delta^2H = 7.2\ [CI\ 6.8; 7.6]\cdot\delta^{18}O + 5[CI\ 2.4; 7.7]$$

slightly different from the data reported by Giustini et al. (2016) ($\delta^2H = 8.04\cdot\delta^{18}O + 11.47$) for North Italy, but similar to a southern site in Austria (Klagenfurt $\delta^2H = 7.8\cdot\delta^{18}O + 7.1$, Hager and Foelsche, 2015). The LMWLs determined over precipitation-weighted year averages ($r^2 = 0.97$; Figure S22e) was very close to the unweighted one:

$$\delta^2H = 7.2\ [CI\ 6.8; 7.6]\cdot\delta^{18}O + 4.5[CI\ 1.6; 7.6]$$

The LMWL computed on all single samples ($n = 1365$, $r^2 = 0.98$; Fig. 8) was:

$$\delta^2H = 7.8\ [CI\ 7.7; 7.9]\cdot\delta^{18}O + 8.9[CI\ 8.3; 9.4]$$

with a prediction error of 3.1‰ δ^2H (5-folds cross-validated RMSE). This value is very similar to $\delta^2H = 7.71\cdot\delta^{18}O + 9.4$ reported by Longinelli and Selmo (2003) for North Italy and calculated over mean monthly samples. The LMWLs calculated at annual and seasonal basis (Fig. 9, black symbols) show smaller slopes (7.1 [CI 6.9;7.3]) and intercepts (4 [CI 2.9;5]) in summer while higher regression coefficients were recorded in winter (slope 8.3 [CI 8.2;8.4]; intercept 13.5 [12.5;14.6]), clearly depicting the seasonal effect over the isotopic composition.

Further, LMWLs were determined for each site using single samples (Table S3). The slopes ranged from 6.9 (Gorizia, ID25) to 8.6 (Zoncolan, ID7), generally showing increasing values with altitude. Similarly, intercepts varied from 2.6‰ (ID25) to 18‰ (ID7), exhibiting increasing values from coastal-plain sites to high-mountain sites. A further regression analysis among slopes (β_1) and intercepts (β_0) (Fig. 9) showed a clear and strong relationship ($r^2 = 0.85$). In addition, the regression coefficients of the single-site LMWLs exhibited similar relationships against the site altitude and the minimum distance from the nearest coast. LMWLs were similar to the GMWL (i.e. slopes close to 8 and intercepts ~ 10) in sites with an altitude between ~ 100 and ~ 1500 m (Figure S23). In these "intermediate sites", the fractionation of the water isotopologues under both equilibrium and non-equilibrium conditions are similar, indicating the stronger influence of water vapor of more local origin.

However, both coefficients drop for sites < 100 m or close to the coastline (<20 km). Generally, slopes below 8 indicate kinetic fractionation due to the secondary evaporation of rainfall, i.e. non-equilibrium isotope exchange occurring when rain droplets fall between the cloud bases to the ground passing through a unsaturated air column. Hence, this effect may explain the drop of both slopes and intercepts for sites in the more flat and coastal areas due to the longer extension of the rainfall path between the cloud bases and the ground (more time for secondary evaporation) as well as to the lower humidity (higher evaporation rate) in the air column with respect to the mountain areas.

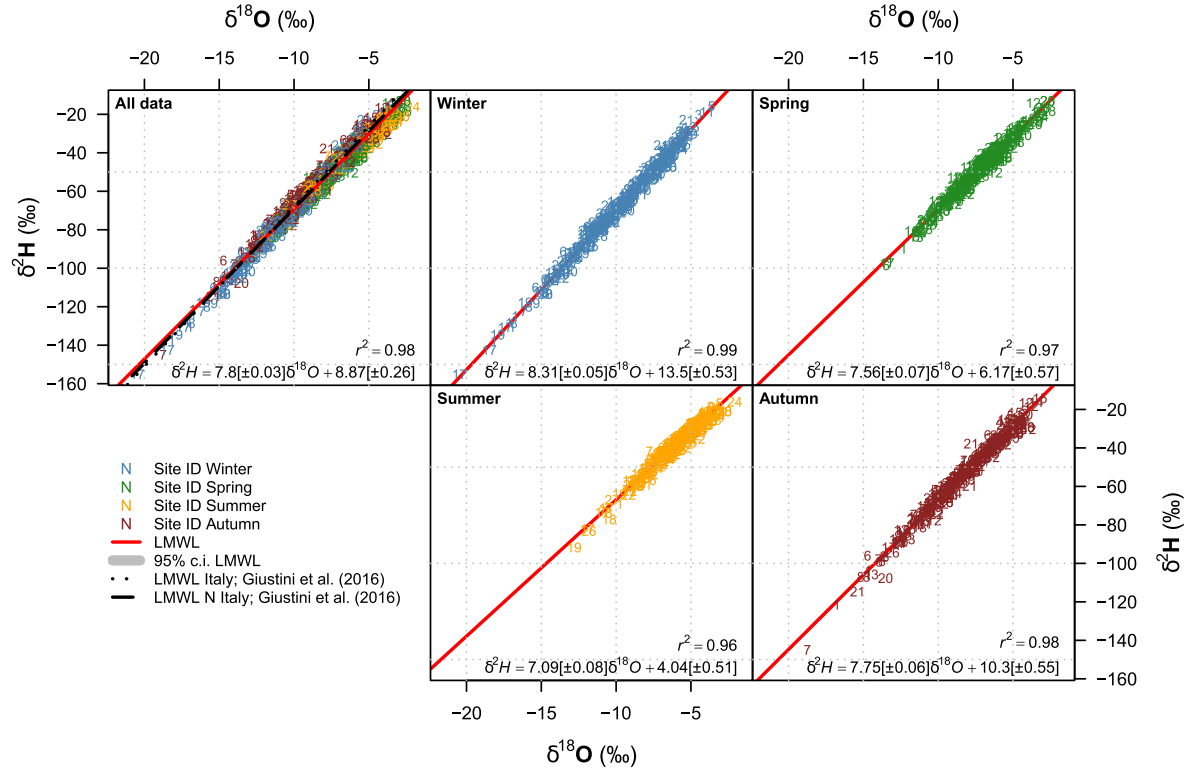

Fig. 8. Local meteoric water lines computed using all the analyzed samples at both annual (all data) and seasonal basis. Regression parameters are also summarized in Table 2. The plot for all data also illustrated in comparison to LMWLs reported by other studies in Northern Italy (for interpretation of the references to color in the figure legend, the reader is referred to the web version of this article).

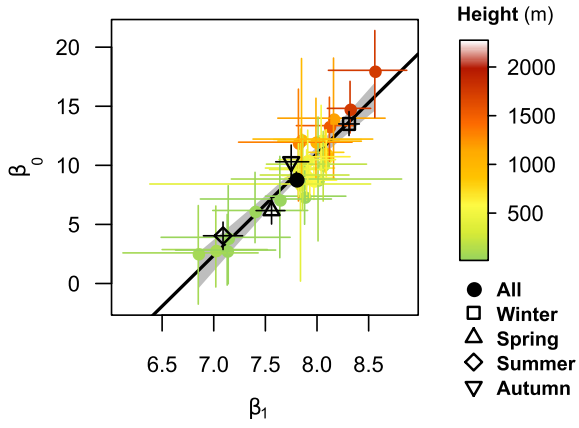

Fig. 9. Relationship between the slopes (β_1) and intercepts (β_0) of the LMWL regression computed for all the sites (colored dots, the color scale shows the altitude of the sampling site). The regression parameters computed over all the sites at annual and seasonal basis are reported as black symbols. The bars represent the 95th confidence intervals of the regression coefficients as estimated by bootstrap (for interpretation of the references to color in the figure legend, the reader is referred to the web version of this article).

Figure S23 also shows that intercepts increase quasi-linearly with the altitude for sites located >~500 m, indicating that topography has an effect on non-equilibrium kinetic fractionation processes. A similar result is reported by Liotta et al. (2006a), who interpreted this behavior by the interaction between falling raindrops and orographic clouds. Hence, high deuterium excess values of the higher sites can be also related to the orographic precipitation with a *seeder-feeder* mechanism.

3.5. Interannual trends

Long-term data sets are useful to detect and quantify possible trends in the delta values or deuterium excess that may be related to changes in the water cycle processes due to recent climate variability (e.g., Stumpp et al., 2014). In this study, four sites present long time-series for $\delta^{18}O$, i.e. >9 years of available data starting in the 90 s (ID 20, 21, 22, 28), while $\delta^{2}H$ and d-excess are generally available starting in 2006 at all the sites. No statistically significant ($p < 0.05$) interannual trends were detected by analyzing the long time-series (not shown) either considering all annual data or single seasons separately and using both raw or deseasonalized data through STL procedure. Statistically significant positive trends ranging from 0.23 to 0.87‰/yr were detected only for d-excess (Table S4). Despite these trends were generally found on the northeasternmost sites (Figure S24), their spatial distribution is neither homogeneous over the study area nor related to the site altitude, indicating that factors driving the trends may be local rather than regional.

3.6. Mapping

The validity of regression models developed to predict the spatial variability over a spatial domain relies on the characteristics and distribution of the points (sites) used for inferring the prediction. In this study, the characteristics of the sites extensively cover the variation of the independent variables across the study area. The spatial extent (latitude, longitude) is well covered by the wide distribution of the sites. The orography is also well represented due to the high density of sites in mountain areas, where there is a larger spatial variability of the altitude. The sites in the mountain areas include valleys, medium-altitude and high-mountain sites. Conversely, the site density is lower to the South; however, the southern part of the region is a flat area with probable little changes in the isotopic composition of precipitation. In addition, four sites are located close to the coastline.

The choice to use the IDW interpolation (power 2) to map the residuals was supported by the Moran's I measure of spatial autocorrelation computed on the residuals of the models. No spatial autocorrelation at alpha = 0.05 was detected (except for d-excess in spring), indicating that residuals are randomly distributed across the domain. Thus, the role of the residuals is emphasized using a deterministic interpolation, allowing to directly detect the sites where local factors have an influence on the isotopic composition of precipitation.

The two modelling approaches were applied using either arithmetic or precipitation-weighted seasonal averages. The selection of the best approach was based on the analysis of cross-validated (CV, 5-fold) RMSE and MAE as estimators for the goodness of the predictions as well as evaluating the presence of patterns in the residuals. Despite the application of the two methods yielded to similar results, the higher R^2 and the lower standard errors of the estimate, CV-RMSE and CV-MAE, were obtained using precipitation-weighted averages and applying the models based on the stepwise regression analysis. This method also provided the less extent of R^2 shrinkage via 5-fold cross-validation (CV R^2). In addition, the VIF quotient analysis did not reveal severe multicollinearity among variables (VIF < 4, tolerance > 0.2). The low effect of collinearity is also reflected by the regression coefficients for the altitude (0.17 $\delta^{18}O_p$‰/100 for all the seasons), revealing values close to the altitude effect reported in the literature for the North Italy (-0.19 $\delta^{18}O$‰/100; Longinelli and Selmo, 2003).

Results are summarized in Table 3, maps in Fig. 10 and maps of residuals in Figures S25-S27. The method was able to explain 68–75% and 60–82% of variances for $\delta^{18}O_p$ and δ^2H_p, respectively. However, the model failed to obtain statistically significant results for the deuterium excess during wintertime, while it was able to explain 50–79% of the variance during the remaining seasons. The poor relation of d-excess with predictors is consistent with the lack of spatial variability already discussed when analyzing the d/ $\delta^{18}O$ ratios for groups of sites located in different areas of FVG (Fig. 7b).

The maps for $\delta^{18}O_p$ and δ^2H_p showed very similar spatial and seasonal patterns. The altitude was the overwhelming predictor mostly shaping the maps (Fig. 10), while latitude and longitude were not always included in the models according to the Akaike information criterion. The analysis of the relative importance metrics for linear models (R^2 partitioned by averaging over orders (Grömping, 2006), showed that where latitude and/or longitude have been included as independent variables, the altitude contribution to R^2 was 64% for $\delta^{18}O_p$ and δ^2H_p, and 79% for d_p, while the contribution of longitude was always lower than 12%. The additional variable T_{diff}, originally included in the models to account for the difference of sampling periods among sites, did not show significant increases in the goodness of fit and was therefore excluded from all the models.

The maps of residuals (Figures S25-S26) showed no spatial patterns and lower values in summer for both for $\delta^{18}O_p$ and δ^2H_p. This finding reflects the lower RMSE assessed through cross-validation, indicating that the model better performed during the summer. On the contrary, higher residues were found in winter and autumn. Since residuals reflect the spatial variability unexplained by the geographic variables, this result confirms that local characteristics and weather conditions have a more important effect on the isotopic composition of precipitation during colder periods. One of the most probable causes of this result is linked to snowfall events: in some mountain sites (e.g., ID8), the experimentally-measured delta values were more depleted than the values predicted by the model, pointing out the possible influence of snow in the isotopic composition of collected samples.

Similarly to Liebminger et al. (2006a), the average of the four seasonal models was used to predict annual results (Figure S28). This choice improved the model performance by including the different influences during the various seasons. Since the deuterium excess was not modelled in winter, indicating a poor spatial variation, the annual mean map of d_p was computed by averaging the maps of the 3 seasons with the average value of d-excess measured over the whole FVG.

This model has the advantage to be simple, including 3 or 4 variables and linear relationships. These simple approaches were selected to obtain a quick prediction of the isotopic composition of precipitation across the region. More sophisticated regression models might be applied to the data using different approaches, including multiple regression analysis with nonlinear terms and the D/S/A (deletion/substitution/addition) algorithm (Sinisi and Van der laan, 2004a; 2004b) and the spatio-temporal bayesian modelling (Bakar and Sahu, 2015). These models will be discussed in a companion paper (Masiol et al., in preparation).

3.7. Comparison with previous data and implication for the regional hydrogeological cycle

The knowledge of the isotopic composition of precipitation allows a comparison with groundwater and thus a better understanding of the hydrological cycle. The isotopic composition of precipitation was therefore compared with data available in the literature for groundwater, surface waters (rivers, lakes), springs and caves. Briefly, Cucchi et al. (2008) analyzed the $\delta^{18}O$ in 128 aquifers in the FVG plain area (72 phreatic, 38 shallow confined, and 18 deep confined). Calligaris et al. (2018) reported the isotopic composition of different hydrogeological compartments, including 4 water caves, 4 wells/piezometers, 4 rivers, 2 lakes and 5 springs in the Classical Karst region aquifer area encompassing the eastern FVG and the Slovenian karstic areas. Martelli and Granati (2010) measured the isotopic composition of 56 wells reaching 8 confined aquifer levels in the low FVG plain multi-layered system as well as the isotopic composition of 17 springs in the spring belt and 4

Table 3
Results of the stepwise regression model. Beta coefficients of multiple regression analysis (β_0 = intercept; β_1 = coefficients) with 95 percentile confidence intervals (CI) estimated by bootstrap and cross-validated (CV, 5-folds) R^2, RMSE and MAE.

Dep. Variable	Season	N	Coefficients				R^2	CV R^2	CV RMSE	CV MAE
			β_0 (±std. error)	$\beta_{Altitude}$ (±std. error)	$\beta_{Latitude}$ (±std. error)	$\beta_{Longitude}$ (±std. error)				
		–	–	*m*	*Decimal degree*[a]	*Decimal degree*[a]		–	*(‰)*	*(‰)*
$\delta^{18}O$	winter	34	124.4 (±32.2)	−0.0016 (±0.0004)	−2.89 (±0.7)	–	0.74	0.64	1.00	0.80
	spring	33	−16.3 (±3)	−0.0016 (±0.0002)	–	0.72 (±0.23)	0.75	0.66	0.60	0.40
	summer	33	−5.5 (±0.1)	−0.0016 (±0.0002)	–	–	0.73	0.65	0.50	0.40
	autumn	34	28.1 (±32.5)	−0.0016 (±0.0004)	−0.94 (±0.65)	0.61 (±0.39)	0.68	0.62	0.90	0.70
δ^2H	winter	28	1052.9 (±258.5)	−0.0109 (±0.0035)	−24.09 (±5.63)	–	0.76	0.67	8.20	6.40
	spring	27	236.8 (±175)	−0.0082 (±0.0024)	−6.12 (±3.81)	–	0.6	0.46	5.90	4.90
	summer	29	2 (±21.1)	−0.012 (±0.0011)	–	−2.63 (±1.58)	0.82	0.74	3.50	2.80
	autumn	29	594.1 (±236.4)	−0.0086 (±0.003)	−13.9 (±5.15)	–	0.63	0.50	7.10	5.40
d	winter	28	–	–	–	–	–	–	–	–
	spring	27	8.3 (±0.3)	0.0026 (±0.0004)	–	–	0.63	0.54	1.20	1.00
	summer	29	15.9 (±5.3)	0.0027 (±0.0003)	–	−0.56 (±0.4)	0.79	0.71	0.90	0.70
	autumn	29	11.3 (±0.4)	0.0025 (±0.0005)	–	–	0.5	0.38	1.50	1.20

a) WGS84 decimal degree, EPSG:4326

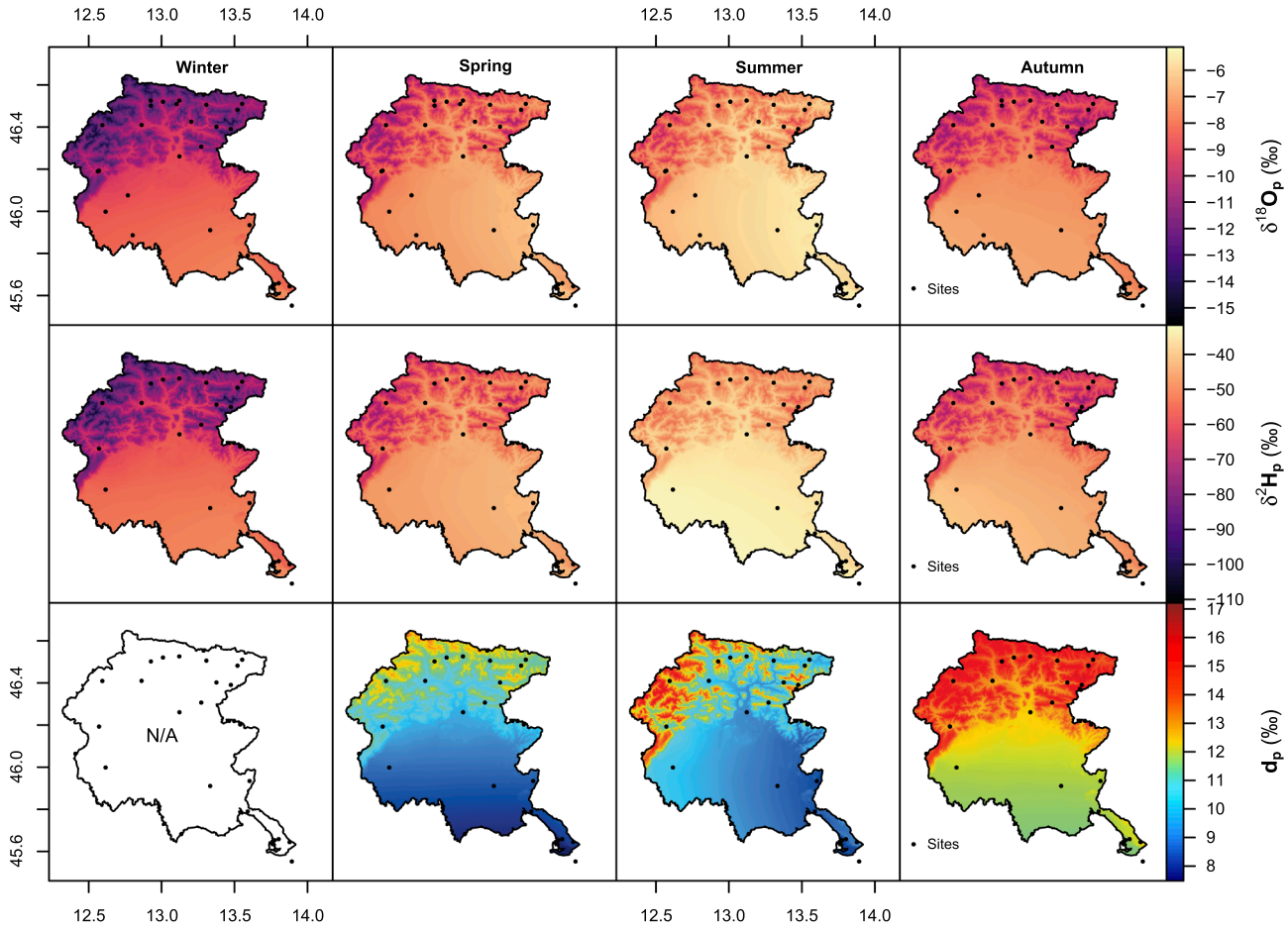

Fig. 10. Map of spatial distribution of $\delta^{18}O$, $\delta^{2}H$, and deuterium excess (all expresses as ‰) of precipitations in FVG. The maps of the spatial distribution of residuals are reported in Figures S25-S27. The maps also report the sites included in the computations (black dots), which may differ among seasons because of data gaps (for interpretation of the references to color in the figure legend, the reader is referred to the web version of this article).

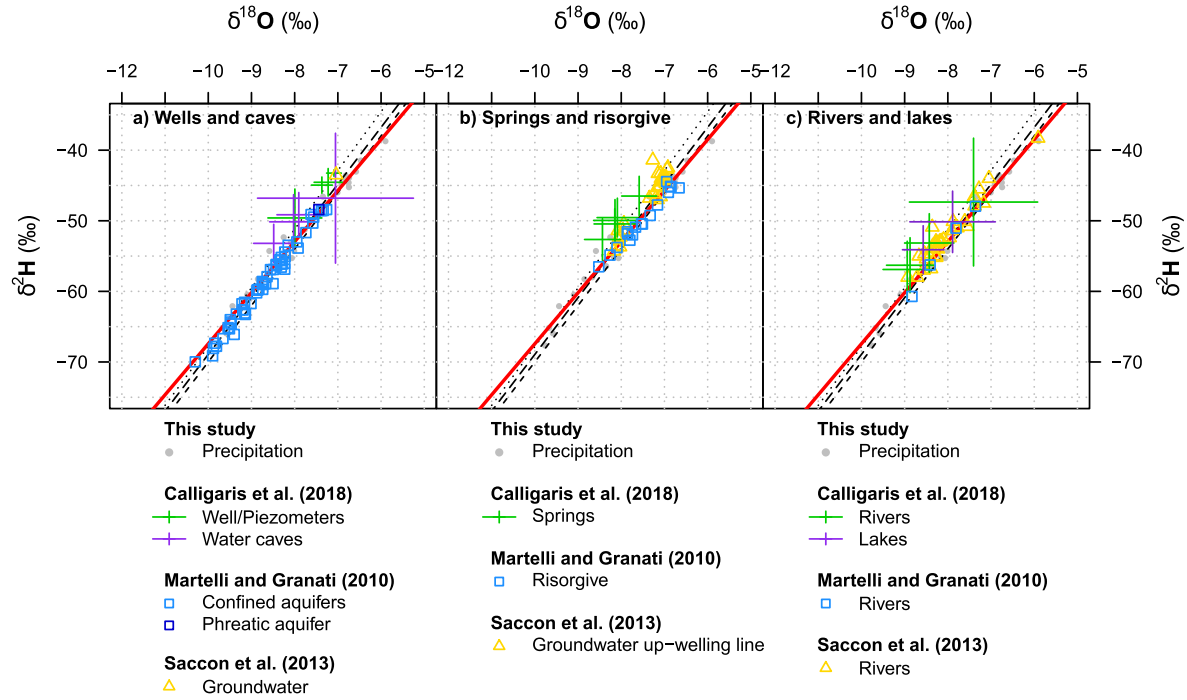

Fig. 11. Comparison between the precipitation-weighted LMWL and the data available in literature. Isotopic data of wells and caves (a), spring water (b) and superficial waters (c) were retrieved from Martelli and Granati (2010), Saccon et al. (2013) and Calligaris et al. (2018).

rivers. Saccon et al. (2013) reported the isotopic composition of a large number of water samples collected in the Lagoon of Marano (located along the southern FVG coastline), its tributary rivers, the spring belt, sewer pipes, and open water from the Adriatic Sea.

$\delta^{18}O$ data presented in the literature for aquifers, rivers, springs and lakes agree with data collected in this study (Figure S29). In particular, the ranges of $\delta^{18}O$ reported in the literature for groundwater and springs fall well within the precipitation-weighted annually-averaged delta values (red boxes) for sites at > 100 m altitude, which mostly correspond to the catchment areas of the confined aquifers. In addition, the $\delta^{18}O$ reported in the literature show a much lower range of isotopic values compared to precipitation monthly samples (grey boxes). This result may indicate that aquifers generally favor the mixing of meteoric waters through the year. On the contrary, less depleted $\delta^{18}O$ values are reported for the Lagoon of Marano, showing intermediate values between the precipitation and the Adriatic Sea (Saccon et al., 2013) due to the mixing of freshwater and seawater.

Inspired by previous studies (e.g., Liotta et al., 2006a, 2013; Paternoster et al., 2008; D'Alessandro et al., 2013), the precipitation-weighted LMWL (Figure S22e) was used to define the meteoric end-members for a direct comparison with the isotopic composition data available in the literature. These values are often recognized to provide good estimations of the isotopic signature for waters that feed aquifers in the Mediterranean area (Liotta et al., 2006a; 2006b; 2013; Paternoster et al., 2008). Results show that the isotopic composition of groundwaters, springs, and superficial waters collected in FVG lies very well along the precipitation-weighted LMWL (Fig. 11). Thus, post-precipitation non-equilibrium fractionation processes (e.g., evaporation at the air–-water interface, evapotranspiration, interaction between water and rocks or biological effects) and the effects of the morphological and hydrogeological parameters of soils and bedrock (e.g., permeability, porosity, slope and soil cover) are negligible and do not change the isotope ratios in other hydrogeological compartments significantly. Under this view, the experimentally measured isotope ratios and maps estimated in this study may be used as geochemical tracers for future hydrological studies.

3.8. Strengths and limitations

This study presents some novel approaches and has several strengths:

1) The sampling density. Generally, studies on water isotopes present poor spatial resolutions, while this study offers a high density of sites that allows a comprehensive understanding of the "medium-scale" changes in the isotopic composition of precipitations.
2) The sampling periods. Sampling sites operated over multiple years, mostly between 2005 and 2012; the sampling frequency was also similar (monthly). This synchronous sampling campaign allows for a better inter-site comparison, not easily achievable when using data from the GNIP or multiple networks.
3) The study area. FVG is largely representative of many continental middle-latitude regions and also presents a complex orography. Such heterogeneous geographic and environmental characteristics (along with the high precipitation rates) makes FVG very interesting for a hydrological point of view with the results largely exploitable to other regions.
4) The chemometric approaches. Generally, studies on the isotopic composition of precipitations rely on basic statistics, often using parametric statistics or non-robust procedures. This study applies more robust statistical approaches (often nonparametric). Also, results of regressions, long-term trends and seasonal patterns are provided with the prediction biases assessed by nonparametric bootstrap resampling.
5) More reliable seasonal amplitudes. Seasonal patterns are often modeled in a simple way or with sine-wave functions. This study applies a seasonal-trend decomposition procedure of time series accounting for preserving the heterogeneous seasonal patterns and better fitting the real data.
6) Summary of a large amount of data. Data of sampling sites are singularly reported but the overall dataset was also comprehensively investigated using clear and synthetic procedures that allow for a broader view of the results and can be of great interest for an international audience.

Beside all these points of strength, this study has some limitations: (i) the lack of a proper snow sampling procedure may lead to bias and artifacts, mostly in high-mountain sites in winter; (ii) the lack of a comprehensive set of weather data to be associated with the isotopic composition of precipitation did not allow to a better model of the spatial and seasonal patterns, as done in previous studies (e.g., Liebminger et al. 2006a); (iii) the lack of concurrent sampling campaign for superficial waters or springs that do not allow for a direct comparison with precipitation data for better investigating the regional hydrogeological cycle (section 3.7).

4. Conclusions

One of the main challenges currently faced by researchers and policymakers is the comprehensive understanding of the hydrogeological cycles over regions where the water resource is threatened by heavy exploitation, pollution, land-use changes, infrastructures, and climate change. In these regions, the identification of recharging catchment basins feeding rivers, aquifers and springs is possible using a reliable geochemical tracer for hydrological studies, like the isotopic composition of water. However, one of the main gaps in water isotopes research is the generally poor spatial resolution of experimental data, which frequently cover large domains with a few sampling points. This poor resolution does not allow for a comprehensive understanding of the "medium-scale" changes in the isotopic composition of precipitations. The present study partially overcomes this limitation providing a high spatially-resolved dataset in the north-easternmost region of Italy. This area can be representative of many continental mid-latitude regions. Given the long-term data and the high density of sites across such complex area from a geomorphological and hydrological point of views, this study provides a solid dataset that is also relevant for other regions where groundwater is a precious and high-quality exploitable resource. This dataset was investigated using both routine and robust approaches which have never been used in isotopic studies.

The average altitude effect was estimated as -0.17 $\delta^{18}O_p$‰/100 m and -1.3 $\delta^{2}H_p$‰/100 m, similar to previous data collected over Northern Italy. The local meteoric water line computed on the original samples was $\delta^2H = 7.8 \cdot \delta^{18}O + 8.9$, while the water line determined over unweighted yearly averages was $\delta^2H = 7.2 \cdot \delta^{18}O + 5$, both very close to the global meteoric water line.

Despite the small extension of the study area, the isotopic composition of precipitation exhibits evident gradients, being more depleted in ^{18}O and ^{2}H from the coastline and flat plain to the northern Alpine area. Seasonal patterns and the amplitude of seasonal isotopic composition of rainfall were investigated using robust statistical approaches. Similar patterns are found in mountain sites experiencing more depleted isotope ratios and more pronounced seasonal variations. The topography of the region determines microclimatic changes in the mountain region that impact on the isotopic composition of precipitations. Evident changes in both slopes and intercepts of the local meteoric water lines are detected. The kinetic fractionation due to the secondary evaporation of rainfall plays an important role in lowering the slopes below 8 in sites located in the flat and coastal areas. On the contrary, intercepts increase quasi-linearly with altitude in mountain sites (>~500 m), indicating that topography may have an effect on kinetic fractionation processes probably related to the orographic precipitation with a *seeder-feeder* mechanism. Despite the spatial variation in the isotopic composition,

the monthly $\delta^{18}O$, $\delta^{2}H$ and deuterium excess are generally well correlated through the entire region even considering "deseasonalized" time-series to drop the effect of seasonality. This is consistent with air masses of similar origin. Two simple methods were applied to predict the isotopic composition of precipitation across the region. Both methods yielded to similar results, serving as a reference for subsequent studies on water resources across FVG. Furthermore, this dataset can be used as a benchmark for numerical models (e.g., trajectories ensemble models) for a deeper understanding of the physical processes driving the isotopic variability of precipitation in the region.

CRediT authorship contribution statement

Mauro Masiol: Conceptualization, Methodology, Software, Validation, Formal analysis, Data curation, Writing - original draft, Writing - review & editing. **Daniele Zannoni:** Conceptualization, Validation, Writing - original draft, Writing - review & editing. **Barbara Stenni:** Conceptualization, Validation, Writing - original draft, Writing - review & editing, Supervision, Funding acquisition. **Giuliano Dreossi:** Conceptualization, Validation, Investigation, Writing - original draft, Writing - review & editing. **Luca Zini:** Investigation, Writing - original draft, Writing - review & editing, Funding acquisition. **Chiara Calligaris:** Investigation, Writing - original draft, Writing - review & editing. **Daniele Karlicek:** Investigation. **Marzia Michelini:** Validation, Investigation. **Onelio Flora:** Investigation, Funding acquisition. **Franco Cucchi:** Funding acquisition. **Francesco Treu:** Investigation.

Declaration of Competing Interest

The authors declare that they have no known competing financial interests or personal relationships that could have appeared to influence the work reported in this paper.

Acknowledgements

Weather data are provided by ARPA FVG – OSMER e GRN (http://www.meteo.fvg.it/). The research has been partially realized in the framework of the projects named Carta Geologico Tecnica (CGT), between Regione Autonoma Friuli Venezia Giulia-Servizio Geologico and Trieste University - DMG. Data on Classical Karst areas have been acquired within the INTERREG ITA-SLO project named HYDROKARST (L'acquifero del Carso quale risorsa idrica strategica transfrontaliera/Kraški vodonosnik kot strateški čezmejni vodni vir). The authors would like to thank all the colleagues, collaborators, and students who helped in logistics and in collecting the samples through the years. The authors would like to thank Marcello Liotta and other two anonymous referees who kindly reviewed the earlier version of this manuscript and provided valuable suggestions and comments.

Appendix A. Supplementary data

Supplementary data to this article can be found online at https://doi.org/10.1016/j.jhydrol.2020.125749.

References

Aemisegger, F., Pfahl, S., Sodemann, H., Lehner, I., Seneviratne, S.I., Wernli, H., 2014. Deuterium excess as a proxy for continental moisture recycling and plant transpiration. Atmos. Chem. Phys. 14, 4029–4054. https://doi.org/10.5194/acp-14-4029-2014.

Affolter, S., Häuselmann, A., Fleitmann, D., Lawrence Edwards, R., Cheng, H., Leuenberger, M., 2019. Central Europe temperature constrained by speleothem fluid inclusion water isotopes over the past 14,000 years. Sci. Adv. 5 https://doi.org/10.1126/sciadv.aav3809.

Aggarwal, P.K., Alduchov, O.A., Froehlich, K.O., Araguas-Araguas, L.J., Sturchio, N.C., Kurita, N., 2012. Stable isotopes in global precipitation: A unified interpretation based on atmospheric moisture residence time. Geophys. Res. Lett. 39 https://doi.org/10.1029/2012GL051937.

Araguás-Araguás, L., Froehlich, K., Rozanski, K., 2000. Deuterium and oxygen-18 isotope composition of precipitation and atmospheric moisture. Hydrol. Process. 14, 1341–1355. https://doi.org/10.1002/1099-1085(20000615)14:8<1341::AID-HYP983>3.3.CO;2-Q.

Bakar, K.S., Sahu, S.K., 2015. spTimer: Spatio-temporal bayesian modeling using R. J. Stat. Softw. 63, 1–32. https://doi.org/10.18637/jss.v063.i15.

Beck, H.E., Zimmermann, N.E., McVicar, T.R., Vergopolan, N., Berg, A., Wood, E.F., 2018. Present and future köppen-geiger climate classification maps at 1-km resolution. Sci. Data 5, 180214. https://doi.org/10.1038/sdata.2018.214.

Benetti, M., Reverdin, G., Pierre, C., Merlivat, L., Risi, C., Steen-Larsen, H.C., Vimeux, F., 2014. Deuterium excess in marine water vapor: Dependency on relative humidity and surface wind speed during evaporation. J. Geophys. Res. 119, 584–593. https://doi.org/10.1002/2013JD020535.

Beniston, M., 2006. Mountain weather and climate: A general overview and a focus on climatic change in the Alps. Hydrobiologia 562, 3–16. https://doi.org/10.1007/s10750-005-1802-0.

Beria, H., Larsen, J.R., Ceperley, N.C., Michelon, A., Vennemann, T., Schaefli, B., 2018. Understanding snow hydrological processes through the lens of stable water isotopes. Wiley Interdiscip. Rev. Water 5, e1311. https://doi.org/10.1002/wat2.1311.

Bershaw, J., 2018. Controls on Deuterium Excess across Asia. Geosciences (Switzerland) 8 (7), 257. https://doi.org/10.3390/geosciences8070257.

Bivand, R., Pebesma, E., Gómez-Rubio, V., 2013. Applied Spatial Data Analysis with R, 2nd ed, Applied Spatial Data Analysis with R. Springer-Verlag, New York, NY, USA. https://doi.org/10.1007/978-0-387-78171-6.

Bivand, R., Keitt, T., and Rowlingson, B., 2019. rgdal: Bindings for the 'Geospatial' Data Abstraction Library. R package version 1.4-8. https://CRAN.R-project.org/package=rgdal.

Bowen, G.J., Good, S.P., 2015. Incorporating water isoscapes in hydrological and water resource investigations. Wiley Interdiscip. Rev. Water 2, 107–119. https://doi.org/10.1002/wat2.1069.

Bowen, G.J., Wilkinson, B., 2002. Spatial distribution of δ18O in meteoric precipitation. Geology 30, 315–318. https://doi.org/10.1130/0091-7613(2002)030<0315:SDOOIM>2.0.CO;2.

Bronić, I.K., Barešić, J., Borković, D., Sironić, A., Mikelić, I.L., Vreča, P., 2020. Long-Term isotope records of precipitation in Zagreb. Croatia. Water (Switzerland) 12. https://doi.org/10.3390/w12010226.

Brunetti, M., Maugeri, M., Monti, F., Nanni, T., 2006. Temperature and precipitation variability in Italy in the last two centuries from homogenised instrumental time series. Int. J. Climatol. 26, 345–381. https://doi.org/10.1002/joc.1251.

Calligaris, C., Boschin, W., Cucchi, F., Zini, L., 2016. The karst hydrostructure of the Verzegnis group (NE Italy). Carbonates Evaporites 31 (4), 407–420. https://doi.org/10.1007/s13146-016-0320-7.

Calligaris, C., Mezga, K., Slejko, F.F., Urbanc, J., Zini, L., 2018. Groundwater characterization by means of conservative (δ18O and δ2H) and non-conservative (87Sr/86Sr) isotopic values: the classical karst region aquifer case (Italy–Slovenia). Geosciences 8(9), 321. https:// doi.org/10.3390/geosciences8090321.

Canty, A., Ripley, B., 2019. boot: Bootstrap R (S-Plus) Functions. R package version 1.3-23. cran.r-project.org/package=boot.

Carslaw, D.C., Ropkins, K., 2012. Openair - An r package for air quality data analysis. Environ. Model. Softw. 27–28, 52–61. https://doi.org/10.1016/j.envsoft.2011.09.008.

Cervi, F., Borgatti, L., Dreossi, G., Marcato, G., Michelini, M., Stenni, B., 2017. Isotopic features of precipitation and groundwater from the Eastern Alps of Italy: results from the Mt. Tinisa hydrogeological system. Environ. Earth Sci. 76 https://doi.org/10.1007/s12665-017-6748-9.

Christner, E., Aemisegger, F., Pfahl, S., Werner, M., Cauquoin, A., Schneider, M., Hase, F., Barthlott, S., Schädler, G., 2018. The Climatological Impacts of Continental Surface Evaporation, Rainout, and Subcloud Processes on δD of Water Vapor and Precipitation in Europe. J. Geophys. Res. Atmos. 123, 4390–4409. https://doi.org/10.1002/2017JD027260.

Cleveland, R.B., Cleveland, W.S., McRae, J.E., Terpenning, I., 1990. STL: A seasonal-trend decomposition procedure based on loess. J. Off. Stat. 6, 3–73. https://doi.org/citeulike-article-id:1435502.

Craig, H., 1961. Isotopic variations in meteoric waters. Science 133, 1702–1703. https://doi.org/10.1126/science.133.3465.1702.

Cucchi, F., Franceschini, G., Zini, L., 2008. Hydrogeochemical investigations and groundwater provinces of the Friuli Venezia Giulia Plain aquifers, northeastern Italy. Environ. Geol. 55, 985–999. https://doi.org/10.1007/s00254-007-1048-4.

Cucchi F., Franceschini G., Zini L. (2008b) Hydrogeology and geochemistry of the Friuli Venezia Giulia Plain alluvial aquifers, northeastern Italy. In: Groundwater: Modelling, Management. Ed. L.F. Konig & J.L. Weiss, p.p. 231-257. ISBN: 978-1-60456-832-5.

D'Alessandro, W., Katsanou, K., Lambrakis, N., Bellomo, S., Brusca, L., Liotta, M., 2013. Chemical and isotopic characterisation of bulk deposition in the Louros Basin (Epirus, Greece). Atmos. Res. 132, 399–410. https://doi.org/10.1016/j.atmosres.2013.07.007.

D'Amelio, L., Flora, O., Longinelli, A., 1994. Environmental isotope data: oxygen isotope concentration in precipitation in N-E Italy (Friuli-Venezia Giulia). Mineral. Petrogr. Acta 37, 113–124.

Dansgaard, W., 1964. Stable isotopes in precipitation. Tellus 16, 436–468. https://doi.org/10.3402/tellusa.v16i4.8993.

Dansgaard, W., Johnsen, S.J., Clausen, H.B., Dahl-Jensen, D., Gundestrup, N.S., Hammer, C.U., Hvidberg, C.S., Steffensen, J.P., Sveinbjörnsdottir, A.E., Jouzel, J., Bond, G., 1993. Evidence for general instability of past climate from a 250-kyr ice-core record. Nature 364, 218–220. https://doi.org/10.1038/364218a0.

Davison, A.C., Hinkley, D.V., 1997. Bootstrap Methods and Their Applications. Cambridge University Press, Cambridge.
Delavau, C., Stadnyk, T., Birks, J., 2011. Model based spatial distribution of oxygen-18 isotopes in precipitation across Canada. Can. Water Resour. J. 36, 313–330. https://doi.org/10.4296/cwrj3604875.
Dinno, A., 2017. dunn.test: Dunn's Test of Multiple Comparisons Using Rank Sums. R package version 1.3.5. https://CRAN.R-project.org/package=dunn.test.
Dütsch, M., Pfahl, S., Sodemann, H., 2017. The impact of nonequilibrium and equilibrium fractionation on two different deuterium excess definitions. J. Geophys. Res. Atmos. 122, 12732–12746. https://doi.org/10.1002/2017JD027085.
Dutton, A., Wilkinson, B.H., Welker, J.M., Bowen, G.J., Lohmann, K.C., 2005. Spatial distribution and seasonal variation in 18O/16O of modern precipitation and river water across the conterminous USA. Hydrol. Process. 19, 4121–4146. https://doi.org/10.1002/hyp.5876.
Epstein, S., Mayeda, T., 1953. Variation of O18 content of waters from natural sources. Geochim. Cosmochim. Acta 4, 213–224. https://doi.org/10.1016/0016-7037(53)90051-9.
Flora, O., Di Varmo, J., Stenni, B., Genoni, L., Carniel, A., 2009. Oxygen isotope composition as a tool for aquifer assessment: The CAMI-Life project case. Boll. Geofis. Teor. Appl. 50, 51–58.
Fox, J., Weisberg, S., 2019. An R Companion to Applied Regression, Third edition. Sage, Thousand Oaks CA. https://socialsciences.mcmaster.ca/jfox/Books/Companion/.
Froehlich, K., Gibson, J.J., Aggarwal, P., 2002. Deuterium excess in precipitation and its climatological significance. J. Geophys. Res. 1–23.
Gat, J.R., 1996. Oxygen and Hydrogen Isotopes in the Hydrologic Cycle. Annu. Rev. Earth Planet. Sci. 24, 225–262. https://doi.org/10.1146/annurev.earth.24.1.225.
Gat, J.R., Mook, W.G., Meijer, A.J., 2001. Environmental Isotopes in the Hydrological Cycle. Principles and Application. Volume II. IHP-V Technical Documents in Hydrology, N° 39. UNESCO – IAEA 2001.
Gat, J.R., Klein, B., Kushnir, Y., Roether, W., Wernli, H., Yam, R., Shemesh, A., 2003. Isotope composition of air moisture over the Mediterranean Sea: An index of the air-sea interaction pattern. Tellus. Ser. B Chem. Phys. Meteorol. 55, 953–965. https://doi.org/10.1034/j.1600-0889.2003.00081.x.
Gat, J.R., 2010. Isotope Hydrology. Imperial College Press, London (UK), A Study of the Water Cycle.
Geyh, M., D'Amore F., Darling, G., Paces, T., Pang, Z., Silar, J., 2001. Environmental Isotopes in the Hydrological Cycle. Principles and Application. Volume IV. IHP-V Technical Documents in Hydrology, N° 39. UNESCO – IAEA 2001.
Giustini, F., Brilli, M., Patera, A., 2016. Mapping oxygen stable isotopes of precipitation in Italy. J. Hydrol. Reg. Stud. 8, 162–181. https://doi.org/10.1016/j.ejrh.2016.04.001.
Gräler, B., Pebesma, E., Heuvelink, G., 2016. Spatio-temporal interpolation using gstat. R J. 8, 204–218. https://doi.org/10.32614/rj-2016-014.
Grolemund, G., Wickham, H., 2011. Dates and Times Made Easy with lubridate. J. Stat. Softw. 40, 1–25. https://doi.org/10.18637/jss.v040.i03.
Gröning, M., Lutz, H.O., Roller-Lutz, Z., Kralik, M., Gourcy, L., Pöltenstein, L., 2012. A simple rain collector preventing water re-evaporation dedicated for δ18O and δ2H analysis of cumulative precipitation samples. J. Hydrol. 448, 195–200. https://doi.org/10.1016/j.jhydrol.2012.04.041.
Grömping, U., 2006. Relative Importance for Linear Regression in R: The Package relaimpo. J. Stat. Softw. 17, 1–27.
Hager B., Foelsche, U., 2015. Stable isotope composition of precipitation in Austria. Austrian J. Earth Sci. 108/2, 2-13. https://doi.org/10.17738/ajes.2015.0012.
Hijmans, R.J., 2019. raster: raster: Geographic data analysis and modeling. R package version 2.1-16. http://CRAN.R-project.org/package=raster.
Holko, L., Dóša, M., Michalko, J., Kostka, Z., Šanda, M., 2012. Isotopes of oxygen-18 and deuterium in precipitation in Slovakia. J. Hydrol. Hydromechanics 60, 265–276. https://doi.org/10.2478/v10098-012-0023-2.
IAEA (International Atomic Energy Agency), 2014. IAEA/GNIP precipitation sampling guide V2. 02 September 2014. Available at: http://www-naweb.iaea.org/napc/ih/documents/other/gnip_manual_v2.02_en_hq.pdf (accessed March 2020).
James, G., Witten, D., Hastie, T., Tibshirani, R., 2013. An introduction to Statistical Learning with Applications in R. Springer, New York, NY, ISBN . 978-1-4614-7138-7. https://doi.org/10.1007/978-1-4614-7138-7.
Jódar, J., Custodio, E., Liotta, M., Lambán, L.J., Herrera, C., Martos-Rosillo, S., Sapriza, G., Rigo, T., 2016. Correlation of the seasonal isotopic amplitude of precipitation with annual evaporation and altitude in alpine regions. Sci. Total Environ. 550, 27–37. https://doi.org/10.1016/j.scitotenv.2015.12.034.
Jouzel, J., Masson-Delmotte, V., Cattani, O., Dreyfus, G., Falourd, S., Hoffmann, G., Minster, B., Nouet, J., Barnola, J.M., Chappellaz, J., Fisher, H., Gallet, J.C., Johnsen, S., Leuenberger, M., Loulergue, L., Luethi, D., Oerter, H., Parrenin, F., Raisbeck, G., Raynaud, D., Schilt, A., Schwander, J., Selmo, E., Souchez, R., Spahni, R., Stauffer, B., Steffensen, J.P., Stenni, B., Stocker, T.F., Tison, J.L., Werner, M., Wolff, E.W., 2007. Orbital and millennial Antarctic climate variability over the past 800,000 years. Science 317, 793–796. https://doi.org/10.1126/science.1141038.
Jurkovšek, B., Biolchi, S., Furlani, S., Kolar-Jurkovšek, T., Zini, L., Jež, J., Tunis, G., Bavec, M., Cucchi, F., 2016. Geology of the classical karst region (SW Slovenia–NE Italy). J. Maps 12 (sup1), 352–362. https://doi.org/10.1080/17445647.2016.1215941.
Kendall, T., 1975. Rank Correlation Methods, 4th ed. Charles Griffin, London, UK.
Klaus, J., McDonnell, J.J., 2013. Hydrograph separation using stable isotopes: Review and evaluation. J. Hydrol. 505, 47–64. https://doi.org/10.1016/j.jhydrol.2013.09.006.
Lai, C.T., Ehleringer, J.R., 2011. Deuterium excess reveals diurnal sources of water vapor in forest air. Oecologia 165, 213–223. https://doi.org/10.1007/s00442-010-1721-2.
Liebminger, A., Haberhauer, G., Varmuza, K., Papesch, W., Heiss, G., 2006a. Modeling the oxygen 18 concentration in precipitation with ambient climatic and geographic parameters. Geophys. Res. Lett. 33 https://doi.org/10.1029/2005GL025049.
Liebminger, A., Haberhauer, G., Papesch, W., Heiss, G., 2006b. Correlation of the isotopic composition in precipitation with local conditions in alpine regions. J. Geophys. Res. Atmos. 111 https://doi.org/10.1029/2005JD006258.
Liotta, M., Favara, R., Valenza, M., 2006a. Isotopic composition of the precipitations in the central Mediterranean: Origin marks and orographic precipitation effects. J. Geophys. Res. Atmos. 111 https://doi.org/10.1029/2005JD006818.
Liotta, M., Brusca, L., Grassa, F., Inguaggiato, S., Longo, M., Madonia, P., 2006b. Geochemistry of rainfall at Stromboli volcano (Aeolian Islands): Isotopic composition and plume-rain interaction. Geochem. Geophys. Geosyst., 7, Q07006, https://doi.org/10.1029/2006GC001288.
Liotta, M., Grassa, F., D'Alessandro, W., Favara, R., Candela, E.G., Pisciotta, A., Scaletta, C., 2013. Isotopic composition of precipitation and groundwater in Sicily. Italy. Appl. Geochem. 34, 199–206. https://doi.org/10.1016/j.apgeochem.2013.03.012.
Longinelli, A., Anglesio, E., Flora, O., Iacumin, P., Selmo, E., 2006. Isotopic composition of precipitation in Northern Italy: Reverse effect of anomalous climatic events. J. Hydrol. 329, 471–476. https://doi.org/10.1016/j.jhydrol.2006.03.002.
Longinelli, A., Selmo, E., 2003. Isotopic composition of precipitation in Italy: A first overall map. J. Hydrol. 270, 75–88. https://doi.org/10.1016/S0022-1694(02)00281-0.
Lykoudis, S.P., Argiriou, A.A., Dotsika, E., 2010. Spatially interpolated time series of δ18O in Eastern Mediterranean precipitation. Glob. Planet. Change 71, 150–159. https://doi.org/10.1016/j.gloplacha.2009.09.004.
Maindonald, J., Braun, J.W., 2010. Data Analysis and Graphics Using R, Third Edition. Cambridge University Press, Cambridge, UK, pp. 565, ISSN 978-0-511-71286-9.
Maindonald, J.H., and Braun, W.J., 2019. DAAG: Data Analysis and Graphics Data and Functions. R package version 1.22.1. https://CRAN.R-project.org/package=DAAG.
Majoube, M., 1971. Fractionnement en oxygene 18 et en deuterium entre l'eau et sa vapeur. Journal de Chimie Physique 68, 1423–1436.
Mann, H.B., 1945. Nonparametric Tests Against Trend. Econometrica 13, 245. https://doi.org/10.2307/1907187.
Martelli, G., Granati, C., 2010. A comprehensive hydrogeological view of the Friuli alluvial plain by means of a multi-annual quantitative and qualitative research survey. Mem. Descr. Carta Geol. d'Italia XC 181–208.
Martelli, G., Granati, C., Toscani, L., Iacumin, P., Selmo, E., 2007. Risultati preliminari delle indagini isotopiche svolte sulle acque delle falde profonde della Bassa Pianura Friulana. Giornale di Geologia Applicata 6, 93–101. https://doi.org/10.1474/GGA.2007-06.0-09.
Masiol M., Zannoni D., Stenni B., Dreossi G., Zini L., Calligaris C., Karliceck D., Michelini M., Flora O., Cucchi F., Treu F., in preparation. Modeling the isotopic composition of precipitations with geographic parameters, modeled and measured weather variables, and land use predictors.
McDermott, F., 2004. Palaeo-climate reconstruction from stable isotope variations in speleothems: A review. Quat. Sci. Rev. 23, 901–918. https://doi.org/10.1016/j.quascirev.2003.06.021.
Michelini, M., 2013. Studio Geochimico-isotopico Delle Precipitazioni Del Friuli-Venezia Giulia. PhD Thesis. Università degli Studi di Trieste.
Mook, W.G, 2001. Environmental Isotopes in the Hydrological Cycle. Principles and Application. Volume I. IHP-V Technical Documents in Hydrology, N° 39. UNESCO – IAEA 2001.
Paradis, E., Schliep, K., 2018. ape 5.0: an environment for modern phylogenetics and evolutionary analyses in R. Bioinformatics 35, 526–528.
Paternoster, M., Liotta, M., Favara, R., 2008. Stable isotope ratios in meteoric recharge and groundwater at Mt. Vulture volcano, southern Italy. J. Hydrol. 348 (1–2), 87–97. https://doi.org/10.1016/j.jhydrol.2007.09.038.
Pebesma, E.J., 2004. Multivariable geostatistics in S: The gstat package. Comput. Geosci. 30, 683–691. https://doi.org/10.1016/j.cageo.2004.03.012.
Penna, D., Stenni, B., Šanda, M., Wrede, S., Bogaard, T.A., Michelini, M., Fischer, B.M.C., Gobbi, A., Mantese, N., Zuecco, G., Borga, M., Bonazza, M., Sobotková, M., Čejková, B., Wassenaar, L.I., 2012. Technical note: Evaluation of between-sample memory effects in the analysis of δ2H and δ18O of water samples measured by laser spectroscopes. Hydrol. Earth Syst. Sci. 16, 3925–3933. https://doi.org/10.5194/hess-16-3925-2012.
Pfahl, S., Sodemann, H., 2014. What controls deuterium excess in global precipitation? Clim. Past 10, 771–781. https://doi.org/10.5194/cp-10-771-2014.
R Core Team, 2019. R: A language and environment for statistical computing. R Foundation for Statistical Computing, Vienna, Austria https://www.R-project.org/.
Rodgers, P., Soulsby, C., Waldron, S., Tetzlaff, D., 2005. Using stable isotope tracers to assess hydrological flow paths, residence times and landscape influences in a nested mesoscale catchment. Hydrol. Earth Syst. Sci. 9, 139–155. https://doi.org/10.5194/hess-9-139-2005.
Rozanski, K., Araguás-Araguás, L., Gonfiantini, R., 1993. Isotopic Patterns in Modern Global Precipitation. Clim. Chang. Cont. Isot. Rec. Geophys. Monogr. Ser. 78 https://doi.org/10.1029/gm078p0001.
Rozanski K., Froehlich, K., Mook, W.G., 2001. Environmental Isotopes in the Hydrological Cycle. Principles and Application. Volume III. IHP-V Technical Documents in Hydrology, N° 39. UNESCO – IAEA 2001.
Saccon, P., Leis, A., Marca, A., Kaiser, J., Campisi, L., Böttcher, M.E., Savarino, J., Escher, P., Eisenhauer, A., Erbland, J., 2013. Multi-isotope approach for the identification and characterisation of nitrate pollution sources in the Marano lagoon (Italy) and parts of its catchment area. Appl. Geochem. 34, 75–89. https://doi.org/10.1016/j.apgeochem.2013.02.007.

Schulte, P., van Geldern, R., Freitag, H., Karim, A., Négrel, P., Petelet-Giraud, E., Probst, A., Probst, J.L., Telmer, K., Veizer, J., Barth, J.A.C., 2011. Applications of stable water and carbon isotopes in watershed research: Weathering, carbon cycling, and water balances. Earth-Science Rev. 109, 20–31. https://doi.org/10.1016/j.earscirev.2011.07.003.

Sen Pranab Kumar, 1968. Estimates of the Regression Coefficient Based on Kendall's Tau. J. Am. Stat. Assoc. 63, 1379–1389.

Sinisi, S.E., Van der laan, M.J., 2004. Loss-based cross-validated deletion/substitution/addition algorithms in estimation. U.C. Berkeley Div. Biostat. Work. Pap Working Pa.

Sinisi, S.E., Van Der Laan, M.J., 2004. Deletion/substitution/addition algorithm in learning with applications in genomics. Stat. Appl. Genet. Mol. Biol. 3 https://doi.org/10.2202/1544-6115.1069.

Sodemann, H., Zubler, E., 2010. Seasonal and inter-annual variability of the moisture sources for alpine precipitation during 1995–2002. Int. J. Climatol. 30, 947–961. https://doi.org/10.1002/joc.1932.

Steen-Larsen, H.C., Sveinbjörnsdottir, A.E., Jonsson, T., Ritter, F., Bonne, J.L., Masson-Delmotte, V., Sodemann, H., Blunier, T., Dahl-Jensen, D., Vinther, B.M., 2015. Moisture sources and synoptic to seasonal variability of North Atlantic water vapor isotopic composition. J. Geophys. Res. 120, 5757–5774. https://doi.org/10.1002/2015JD023234.

Stenni, B., Curran, M.A.J., Abram, N.J., Orsi, A., Goursaud, S., Masson-Delmotte, V., Neukom, R., Goosse, H., Divine, D., Van Ommen, T., Steig, E.J., Dixon, D.A., Thomas, E.R., Bertler, N.A.N., Isaksson, E., Ekaykin, A., Werner, M., Frezzotti, M., 2017. Antarctic climate variability on regional and continental scales over the last 2000 years. Clim. Past 13, 1609–1634. https://doi.org/10.5194/cp-13-1609-2017.

Stumpp, C., Klaus, J., Stichler, W., 2014. Analysis of long-term stable isotopic composition in German precipitation. J. Hydrol. 517, 351–361. https://doi.org/10.1016/j.jhydrol.2014.05.034.

Theil, H., 1992. A Rank-Invariant Method of Linear and Polynomial Regression Analysis. In: Henri Theil's Contributions to Economics and Econometrics. Springer, Dordrecht, pp. 345–381. https://doi.org/10.1007/978-94-011-2546-8_20.

Toreti, A., Fioravanti, G., Perconti, W., Desiato, F., 2009. Annual and seasonal precipitation over italy from 1961 to 2006. Int. J. Climatol. 29, 1976–1987. https://doi.org/10.1002/joc.1840.

Uemura, R., Matsui, Y., Yoshimura, K., Motoyama, H., Yoshida, N., 2008. Evidence of deuterium excess in water vapor as an indicator of ocean surface conditions. J. Geophys. Res. Atmos. 113 https://doi.org/10.1029/2008JD010209.

van der Veer, G., Voerkelius, S., Lorentz, G., Heiss, G., Hoogewerff, J.A., 2009. Spatial interpolation of the deuterium and oxygen-18 composition of global precipitation using temperature as ancillary variable. J. Geochemical Explor. 101, 175–184. https://doi.org/10.1016/j.gexplo.2008.06.008.

Venables, W.N., Ripley, B.D., 2002. Modern Applied Statistics with S, Fourth Edition. NY, USA, Springer, New York.

Vreča, P., Bronić, I.K., Horvatinčić, N., Barešić, J., 2006. Isotopic characteristics of precipitation in Slovenia and Croatia: Comparison of continental and maritime stations. J. Hydrol. 330, 457–469. https://doi.org/10.1016/j.jhydrol.2006.04.005.

Vreča, P., Brencic, M., Leis, A., 2007. Comparison of monthly and daily isotopic composition of precipitation in the coastal area of Slovenia. Isotopes Environ. Health Stud. 43, 307–321. https://doi.org/10.1080/10256010701702739.

Vreča, P., Krajcar Bronić, I., Leis, A., 2011. Isotopic composition of precipitation in Portorož (Slovenia). Geologija 54 (1), 129–138. https://doi.org/10.5474/geologija.2011.010.

Vreča, P., Bronić, I.K., Leis, A., Demšar, M., 2014. Isotopic composition of precipitation at the station Ljubljana (Reaktor), Slovenia–period 2007–2010. Geologija 57 (2), 217–230. https://doi.org/10.5474/geologija.2014.019.

Vreča, P., Krajcar Bronić, I., Leis, A., 2015. Isotopic composition of precipitation at the station Portorož, Slovenia-period 2007–2010. Geologija 58, 233–246. https://doi.org/10.5474/geologija.2015.019.

Wickham, H., 2007. Reshaping data with the reshape package. J. Stat. Softw. 21.

Wickham, H., 2011. The Split-Apply-Combine Strategy for Data Analysis. J. Stat. Softw. 40.

Zeileis, A., Grothendieck, G., 2005. Zoo: S3 infrastructure for regular and irregular time series. J. Stat. Softw. 14.

Zini, L., Calligaris, C., Treu, F., Zavagno, E., Iervolino, D., Lippi, F., 2013. Groundwater sustainability in the Friuli Plain. AQUA mundi 41 – 54. https://doi.org/ 10.4409/Am-058-13-0051.

Zini, L., Casagrande, G., Calligaris, C., Cucchi, F., Manca, P., Treu, F., Zavagno, E., Biolchi, S., 2015. The Karst Hydrostructure of the Mount Canin (Julian Alps, Italy and Slovenia). In: Andreo B., Carrasco F., Durán J., Jiménez P., LaMoreaux J. (eds) Hydrogeological and Environmental Investigations in Karst Systems. Environmental Earth Sciences, vol 1. Springer, Berlin, Heidelberg. https://doi.org/10.1007/978-3-642-17435-3_24.